418

Status of Development and Field Test Experience with High-Temperature Superconducting Power Equipment

Working Group
D1.15

June 2010

Status of Development and Field Test Experience with High-Temperature Superconducting Power Equipment

Working Group

D1.15

Members

Hitoshi Okubo, Convenor (JP), Mathias Noe Secretary (DE), Jeonwook Cho (KP), Alex Malozemoff (US), Luciano Martini (IT), Shigeo Nagaya (JP), Frank Schmidt (DE), Christof Sumereder (AT), Pascal Tixador (FR), Bernd Wacker (DE), Alan Wolsky (US)

ISBN: 978- 2- 85873- 105-3

Table of contents

Executive Summary

By shifting the target of research and development from low temperature superconductivity (LTS) to high temperature superconductivity (HTS), HTS superconductivity (SC) power applications have been nearing the next stage of development. They are now at a practical level of application with prototypes and field tests, etc. In recent years, Bi-based HTS development has reached a practical use and YBCO-based HTS has become a main target for HTS power developments and applications.

As for HTS power applications, research and development include almost all power transmission and distribution equipment, such as cables, transformers, fault current limiters (FCL), rotating machines, magnetic energy storage (SMES), and so on; most of these are AC applications. Conventional functions will be extended with new SC functions. Common development features include HTS material development, such as higher critical current (Ic) and current density (Jc), low AC loss applications, cost reductions, compact size development, etc. In addition, as for common features among the equipment, cooling and electrical insulation are the most critical techniques to be resolved. Cooling techniques will directly contribute to above mentioned high Ic and Jc development, cost and size reduction performances.

Conversely, electrical insulation will be a key common factor in the development of HTS power equipment and will contribute to size reduction, cost reduction, low loss applications, etc. Especially, because dielectric breakdown (BD) constitutes a fatal failure of this type of equipment, electrical insulation performance will be understood as critical for actual power applications. In recent years, worldwide HTS development projects have had a tendency to enhance operational voltage to become as high as conventional voltage, such as at the 145-300kV level.

Under such situations and considering the status of development, HTS power applications are nearing prototype and field tests stages, leading to practical operations in the near future. In this report, state-of-the-art HTS development will be summarized and results of the prototype development and field tests will be introduced for the discussion of future HTS applications. In particular, technical views from both common techniques and peculiar techniques are based on individual equipment and systems, and are described in this brochure.

The Technical Brochure (TB) introduces and discusses worldwide field-test experiences and state-of-the-art HTS power applications.

Chapter 1: The aims of the technical brochure are described and introduced.

Chapter 2: The development status of HTS materials including Bi-based 1st generation and YBCO coated conductor 2nd generation HTS materials are introduced and summarized, including wires, bulk materials, etc.

Chapter 3: The development and test results involving large SC rotating machines with 5-36MVA ship propulsion motors, 8MVA synchronous condenser, 4 MVA generator, etc. are reported, and the newest innovations are introduced.

Chapter 4: HTS power cables with worldwide field test experiences including different concepts, applications and functions are summarized and discussed, as well as the newest innovations. HTS cables with a higher voltage, larger capacity, lower loss, and longer length are introduced.

Chapter 5: The development status of SC fault current limiters (SCFCL) is described using field test results from different current limiting concepts. The state-of-the-art SCFCL is generally investigated and the development of current limiting transformers (SFCLT) is reported.

Chapter 6: The SC magnetic energy storage (SMES) for different applications of power systems is introduced. The field-test results from actual power systems are analyzed and the performances are summarized.

Chapter 7: Concerning common technologies for HTS power applications, the role of electrical insulation performance can be critical, especially for future higher voltage application in HTS power equipment. Both the fundamental and actual field design criteria and concepts are introduced.

Finally, items studied by CIGRE SC D1 WG15 are briefly summarized in Chapter 8. The obtained results can contribute and will be useful to the future development of HTS power equipment and its operation in electric power systems.

Keywords: High temperature superconductivity (HTS), Power applications, Power cable, Rotating machine, Fault current limiter (FCL), Magnetic energy storage (SMES), Electrical insulation, HTS material development, Field test

1 Introduction

Since the discovery of high temperature superconductivity in 1986 by Karl Müller and Georg Bednorz [1.1], considerable progress has been made to develop superconducting large scale equipment [1.2], [1.3] and applications for power systems (e.g. rotating machines [1.4], cables [1.5], transformers [1.6], current limiters [1.7], magnetic energy storage [1.8]). Many successful large scale demonstrator and prototype tests have already underlined the superior performance of high temperature superconductor technology. In addition, the rapid progress in the development of the so-called 2nd generation high temperature superconductor wire [1.9] gives promise to beat the cost-performance ratio of copper in the near future.

A high temperature superconductor (HTS) wire can carry more than 100 times the current density of copper with negligible DC resistance. In general, this leads to much smaller and lighter equipment with higher efficiency. Moreover, superconductivity adds new functions to the grid like fault current limitation.

To penetrate the market, superconductor equipment has to demonstrate at least the same reliability and availability as conventional counterparts. This is best done in long-term field tests. Up to now, no report or publication has summarized the field test experience for a broad range of HTS power equipment for the electric power grid. This is the goal of the present report. The present status of development and state-of-the-art of HTS electric power applications is also described.

Since the HTS material is a key element for each application, the first chapter describes the state-of-the-art of HTS material development. The following chapters deal with HTS rotating machines, cables, fault current limiters and magnetic energy storage systems. Except for a brief section on fault-current-limiting transformers, HTS transformers are not included in this report because these devices have not reached the level of maturity to enter in-grid field tests; particularly the lack of a practical conductor with low AC loss in perpendicular fields limits HTS transformer efficiency.

All components and equipment in power systems need a reliable electrical insulation system up to very high voltages. Therefore, the final chapter presents an overview of the main electrical insulation issues for HTS power equipment.

Many different projects on HTS power equipment have been performed since the discovery of high-temperature superconductivity in 1986. This report does not pretend to give a complete overview of all activities. It concentrates on the most recent activities and on the large scale efforts where HTS equipment for the electrical power grid has achieved field testing.

2 High Temperature Superconductor (HTS) Materials

2.1 State-of-the-Art of HTS Material Development

2.1.1 Bi-2223: "First Generation HTS Wire"

The high temperature superconductor $(Bi,Pb)_2Sr_2Ca_2Cu_3O_{10}$, commonly called Bi-2223, is used in first generation (1G) HTS wire, which is composed of 30-40% Bi-2223 by volume embedded as fine filaments in a silver or silver alloy matrix (see Fig. 2.1) [2.1]. It is produced by a powder-in-tube drawing, rolling and annealing process. For some applications, the wire is laminated to stainless steel, copper or brass tapes on both sides for enhanced mechanical properties and protection from the environment. The wire is a flat tape-shaped product. Its standard dimensions are 0.2-0.3 mm by 4-4.4 mm. World-wide gross production capacity is of order one million meters per year.

Fig. 2.1: Cross-section of 1 G HTS wire, showing 55 filaments (black) embedded in silver, laminated on both sides by stainless steel. (Courtesy of American Superconductor)

Several 1G HTS wire designs are available to meet the requirements of various applications. Depending on the architecture and alloy composition, the wire's critical stress at room temperature can vary from 65 to 265 MPa, critical tensile strain (77K) from 0.3-0.4%, critical compressive strain (77 K) from 0.15-0.25% and minimum bend diameter down to 50 mm for laminated wire [2.2].

The critical current I_c of 1G HTS wire has been a focus of R&D efforts since 1989. The latest significant progress has been achieved by Sumitomo Electric with a high pressure reaction process called CTOP, which has yielded over 200 A in end-to-end I_c at 77 K and self-field (sf) in 0.21 x 4.2 mm long length wire [2.2]. The maximum critical current corresponds to an engineering critical current density J_e of close to 23,000 A/cm^2, and a superconductor current density J_c close to 75,000 A/cm^2. Bi-2223 wire also shows good performance in higher magnetic fields at lower temperatures. For example, at a temperature of 30 K and 2 T perpendicular to the wire plane, the current density of typical 1G HTS wire is about double the 77 K (sf) current density.

1G HTS wire has achieved performance levels required for commercial applications and has been used for the majority of HTS applications prototypes so far, including power cables, motors, generators, synchronous condensers, transformers, and magnets or various kinds [2.3]. Nevertheless there is significant controversy about the future of 1G HTS wire in the context of rapid progress on 2G HTS wire which is claimed to have significantly lower manufacturing costs. Cost has in fact been the principal obstacle to the commercial adoption of 1G HTS wire. For these reasons, a leading HTS wire manufacturer, American Superconductor, has terminated production of 1G HTS wire, although as of 2009 it is still selling from its inventory. Sumitomo Electric in Japan, Bruker HTS (Bruker Advanced Supercon) in Europe and InnoST in China are the principal remaining producers worldwide.

2.1.2 Bi-2212 Wire

Bi-2212 ($Bi_2Sr_2Ca_1Cu_2O_8$) round wires of high critical current density in high magnetic field have been developed [2.4-2.5] They can carry more than 200 kA/cm^2 in a

magnetic field of 10 T and 180 kA/cm^2 in a magnetic field of 20 T at 4.2 K, which exceeds the current-carrying capability of all conventional metallic superconductors.

The round wires are sufficiently ductile to allow cabling. 500 m long 1+6 type stranded cables for large-scale superconducting equipment [2.6] have been manufactured successfully, as shown in Fig. 2.2. They consist of a single Ni-based reinforcement wire surrounded by six Bi-2212 round wires. The I_c value of these cables was 2.5 kA at 4.2 K in self field.

Moreover, Rutherford type cables using Bi-2212 round wires have been manufactured, as shown in Fig. 2.3. [2.7]. The maximum current-carrying capacity achieved to date is 12,000 A at 4.2 K in a back-up field of 0.6 T. An optimised production process has been developed at SWCC Showa Holdings and stranded cable has been delivered for a Japanese SMES project. It is not clear at this time whether the market is developing sufficiently to sustain production capability at SWCC Showa Holdings, the world's only remaining producer of this type of HTS wire. Nexans SuperConductors GmbH has also produced a powder-in-tube tape-shaped Bi-2212 wire which has been used for applications such as a French SMES project.

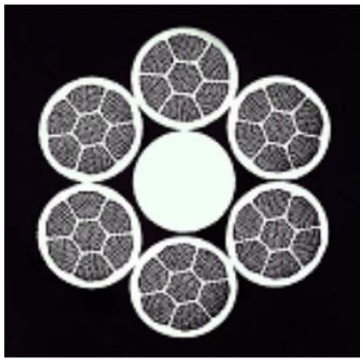

Fig. 2.2: Bi 2212 stranded cables with Ic=2.5 kA at 4.2 K, self field.

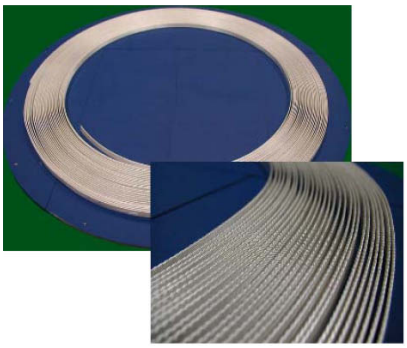

Fig. 2.3: 0.8mm, 30strand Rutherford cable with 70 m length.

2.1.3 Bi-2212 Bulk Material

BSCCO-2212 bulk materials were developed for application in fault current limiters, current leads, hysteresis or reluctance type motors, and levitation applications. Bulk materials typically come in the shape of rings, plates, rods or pellets. They can be produced using pre-reacted powders by solid-state sintering followed by partial melt processing (PMP) or directly from raw oxides by melt cast processing (MCP) [2.8-2.9].

Solid-state sintered BSCCO-2212 is not suitable for high-current applications at 77 K, providing neither good texture nor connectivity between the grains; the technique considered most suitable for needed densification and at least local texturing of BSCCO-2212 is partial melt processing (PMP). In the standard PMP route, the material is heated above the temperature of BSCCO-2212 melting decomposition and then cooled down to reform well connected and textured BSCCO-2212 phase [2.8]. The shape conservation during melting restricts the geometry of final product to millimeter diameter fibers (laser floating zone, LFZ, method [2.10]) or to thin plates/thick films on inert substrates (static PMP [2.11]).

The critical current density is affected by many processing variables, but is principally dependent on the texture of BSCCO-2212 that is induced either by a thermal gradient upon solidification (LFZ method) or by heterogeneous nucleation at the

BSCCO/substrate interface (static PMP). In the latter case, the texture is strongly deteriorated with increasing thickness, which results in strong thickness dependence of j_c(77 K, sf) that decreases from >10 kA/cm^2 in excellently aligned thin (< 20μm) films on Ag substrates to 6–8 kA/cm^2 in thicker (100 μm) films, and to 3 kA/cm^2 in thick (200–600 μm) films [2.12]. The uniformity of texture in thick (0.2–3 mm) films/plates can be improved by solidification in an external magnetic field [2.13], or by introducing aligned MgO fibers inside the pressed plates for heterogeneous nucleation [2.14]. Optimizing oxygen content and maintaining its uniformity over the thickness is an important issue [2.15], as such uniformity is difficult to achieve in well textured bulk material without changing oxygen partial pressure upon cooling [2.14]. The critical temperature for PMP bulk BSCCO-2212 ranges from 85 to 92 K. The achievable average j_c (77 K, sf) in final (decimeter large) products is 2–5 kA/cm^2 and I_c ~ 1 kA. The good texture of partially melt processed BSCCO2212 reduces the normal-state resistivity (usually by an order of magnitude, e.g., ρ_N(300 K) ~ 1 mOhm [2.10]), which limits applicability of partially melt processed BSCCO-2212 bulk in fault current limiter devices.

Melt cast processed (MCP) BSCCO-2212 offers a better combination of critical current density and resistivity for fault current limiter application. In the MCP method, the material is completely melted in Pt crucibles at 1100-1150°C and then cast into different shapes: plates, rods, or tubes (the latter is done using rotating molds). The shape flexibility is indeed a big advantage of the MCP route [2.16]. Though the as-cast state does not contain the BSCCO-2212 phase and is a mixture of four different phases, the subsequent heat treatment that involves partial melting of eutectic allows good equilibration. The BSCCO-2212 phase in the final product is not textured, though local 3D correlations in grain alignment exist on a 100 μm scale. The T_c up to 94.5 K can be optimized by a proper choice of the overall composition [2.17] that (contrary to the PMP route) is not limited to the BSCCO-2212–liquid equilibrium. All these features finally yield a rather good combination of j_c (77 K, sf) ~ 1–4 kA/cm^2 and resistivity ρ_N (300 K) ~ 3–6 mOhm cm, making the material suitable for applications in higher electric fields than PMP BSCCO-2212.

Both PMP and MCP materials are widely used as current leads [2.18], being to some extent complementary with respect to both geometry (millimeter diameter fibers produced by LFZ vs 5-15 mm diameter MCP rods and 26 up to 200 mm diameter MCP tubes) and currents (0.03-1 kA in PMP vs 0.2 to 20 kA in MCP) [2.10, 2.18]. Excellent contacts to Ag, an essential condition for all transport applications, have been realized. Silver paint or metal foil is applied before the final annealing step. On the resulting surface other metals such as copper or brass can then be easily soldered with overall contact resistances below 1 μOhm cm² [2.19].

Produced in up to half meter sizes, the BSCCO-2212 bulk can then be machined to yield ~50 m long conductors suitable to transport applications, in particular, in FCLs. The remaining granularity, in general considered as a disadvantage of the material, is actually used for a novel protection mechanism in FCL devices [2.20] against formation of hot spots. The granularity results in a strong dependence of transport current density on an external magnetic field. Indeed at 77 K j_c decreases by one order of magnitude in a field as small as 0.1 T. The new concept consists of a normal conducting coil wound around the superconductor and connected in parallel. In the case of overcurrent, a voltage along the superconductor appears and drives a current through the normal coil. The resulting field then brings the still superconducting parts of the sample to a fast and homogeneous quench.

Though the BSCCO-2212 bulk materials are always thought to be compromised by their mechanical properties, suitable reinforcement made possible very successful FCL projects for 6 kV [2.21] 10 kV [2.18] and 14 kV [2.22] levels. For distribution level FCLs, the BSCCO-2212 elements are now reaching the commercial level.

2.1.4 YBCO Coated Conductor: "Second Generation HTS Wire"

Second generation (2G) HTS wire is based on the high temperature superconductor $YBa_2Ca_3O_7$, commonly called YBCO. YBCO is deposited as an epitaxial thin film on a flexible highly biaxially textured substrate in such a way that grain boundary limitations to current flow are largely avoided [2.1]. The prospect for low cost manufacturing, and rapid technical progress leading to high critical currents and over 1000 m lengths of tape-shaped wire, have made 2G HTS wire the favoured follow-on to 1G HTS wire for most applications.

2G wire comprises 1) a biaxially-textured template consisting of a tape-shaped metal substrate with multiple buffer layers, 2) an epitaxial YBCO layer applied to the template, 3) a thin silver passivation layer and 4) a thick electrical and mechanical stabilization layer which also provides environmental protection. The final wire product is typically 0.15-0.30 mm thick, and 4-12 mm wide; at 0.3 mm x 4.4 mm, it is a form-fit-function replacement for 1G wire. An example of a cross-section is shown in Fig. 2.4; the configuration is similar to that of 1G wire (Fig. 2.1), but with far less HTS material, located in the dark line separating the central insert and the upper laminate. 2G wire is currently under active development and scale-up in a number of laboratories and companies around the world, and three companies, American Superconductor, SuperPower and Bruker HTS have already initiated commercial sales. As of 2009, availability is beginning to match and even exceed 1G HTS wire availability. Both American Superconductor and SuperPower are scaling up and claim imminent gross capacity close to 1 million meters of 4 mm wide wire per year [2.23, 2.26].

Multiple 2G manufacturing processes are in use or under development at the present time. The two most successful template processes are Rolling Assisted Bi-axially Textured Substrate (RaBiTS^{TM}), in which texturing is achieved directly in the substrate, and Ion-Beam-Assisted Deposition (IBAD), in which texture is achieved in a deposited layer on a non-textured substrate. The three most successful HTS coating processes are Metal-Organic Deposition (MOD) – a liquid phase chemical technique, Metal-Organic Chemical Vapor Deposition (MOCVD), and Pulsed Laser Deposition (PLD) [2.1].

A major driver for 2G wire is the prospect of 2-5 times lower manufacturing cost than 1G. One cost

Fig. 2.4: Cross-section of a 4.4 mm wide laminated wire, called 344 superconductors by American Superconductor, showing three layers: two copper laminates on the top and bottom, and a central insert consisting of a NiW substrate coated with here-invisible buffer and HTS layers. (Courtesy of American Superconductor)

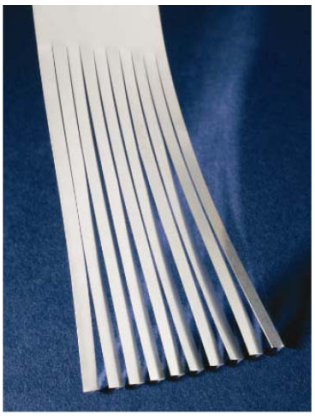

Fig. 2.5: 4 cm wide insert tape slit into 4 mm wide final wire insert (before lamination) (Courtesy of American Superconductor)

advantage comes from the ability to process in wide sheets and slit to final size, as illustrated in Fig. 2.5 [2.24]. Rolling processes like RABiTS for the substrate, liquid phase chemical techniques like MOD for the HTS layer, and solder-lamination for the stabilizer are also expected to be low cost. However, arguments for low cost are also made for the other industrially developing processes.

Because the tapes can be prepared in a variety of widths (e. g. American Superconductor is producing 4 cm wide tapes, then slitting to final width), it is convenient to use amperage per width as a performance metric. In short R&D samples, a world record 1400 A/cm-width at 75 K has been reported by Los Alamos National Laboratory, using a multilayer PLD process [2.24]. Values up to 735 and 803 A/cm-width at 77 K have been achieved in short length samples, respectively, by ISTEC SRL with MOD [2.25] and SuperPower with MOCVD [2.26]. These levels compare to levels of about 500 A/cm-width on Sumitomo Electric's 200 A, 4 mm wide 1G HTS wire [2.2].

Progress in longer length production wire is also rapid around the world. SuperPower has reported a minimum 153 A/cm-width in a 1311 m wire and 362 A/cm-width in a 103 m wire with MOCVD [2.26], American Superconductor – 350 A/cm-width in a 94 m wire and 253 A/cm-width in a 520 m wire with MOD [2.23], SWCC-Showa – 201 A/cm-width in 200 m with MOD [2.27], ISTEC-SRL 212 A/cm-width in a 245 m wire with PLD [2.26], Fujikura – 350 A/cm in a 500 m wire with PLD, and Bruker HTS 253 A/cm-width in 100 m with PLD [2.28]. Sumitomo Electric, Nexans, Chubu Electric Power, Zenergy and SuNAM (Korea) are also active in 2G HTS scale-up. Stabilization of these wires has been achieved with either thick (~10 micron) deposition of silver (most Japanese and European results [2.25, 2.28]), lamination of copper, brass or stainless steel tapes by American Superconductor [2.23], or electrodeposition of copper by SuperPower [2.26].

Mechanical properties of 2G wire are generally superior to those of 1G HTS wire, especially in bending, where the thinness is a major advantage. The high j_c and thin superconducting layer in 2G wire are expected to also enable lower alternating current (AC) losses for applied fields in the plane of the tape.

The recent commercial availability of 2G HTS wire has already enabled the first applications prototypes. A major focus has been on fault current limiters (FCL), enabled by 2G's major reduction in the amount of shunting high conductivity silver as compared to 1G HTS wire and the use of a stainless steel laminate for stabilization. In January 2007, Siemens and American Superconductor announced the successful test of a one phase 13 kV class 2.25 MVA fault current limiter based on 2G wire [2.29], and Hyundai announced a similar test on a 23 kV-class 8.3 MVA system in Korea [2.30]. In late 2008, Siemens and American Superconductor announced a further 13 kV class FCL demonstration, now using an optimised 1 cm wide wire. In June 2007, Nexans and American Superconductor announced fabrication and successful test of a 30 m 138 kV 2G cable [2.31], in March 2009, Bruker HTS, Nexans and their collaborators announced a successful 30 m distribution-level 2G cable under the European Super3C project [2.39], and in 2008, and in 2008, Sumitomo Electric and Furukawa Electric announced a successful 30 m distribution-level 2G cable under a NEDO/METI project in Japan [2.40]. SuperPower has delivered 10 km of 2G HTS wire to Sumitomo Electric which has fabricated a 30 m cable put into in-grid service for several months as part of the DOE Albany cable project [2.32]. The wires in these cable prototypes were stabilized with copper. Several new cable and fault current limiter projects with 2G HTS wire have been recently announced. For example, a superconducting fault current limiting

transformer (SFCLT) project with 2MVA/22kV in Nagoya University has used 270 m length 2G HTS wire for the primary winding and 1150 m length 1G HTS wire for the HV winding

2.1.5 Magnesium Diboride

Since 2001, when the Akimitsu group in Japan discovered superconductivity at up to 40 K in magnesium diboride [2.33], active work around the world has led to long length wires with a powder in tube process at the National Institute for Materials Science and Hitachi Research in Japan [2.34], Los Alamos National Laboratory in the U.S. [2.35], and commercially by Hypertech in Columbus OH and Columbus Superconductor in Genoa, Italy [2.36]. A key feature of such wires is expected to be low cost. Significant progress is also being made in improving pinning properties and achieving high irreversibility fields, using dopants such as SiC [2.37]. Because of the relatively low T_c compared to the cuprate superconductors, this material is more actively considered for magnet applications such as for MRI, rather than for electric power applications.

However, several projects are already considering the use of MgB_2 for FCL [2.38] and potentially for coils in rotating machinery. The real impact of MgB_2 on power devices will become clearer in the near future, when the material will be developed in wires with optimal properties for these applications, such as low AC losses by very fine filaments, and short twist pitch. The possible advantage of using MgB_2 in place of 2G HTS will be determined by studying the best compromise between wire availability in long lengths, wire performance and cost, and operating temperature.

2.2 Conclusions

Superconducting materials for wire-based power applications are making rapid progress, and prototypes based on these materials are at commercial levels. Active competition continues between different materials, and different forms of these materials; the long-term winners are not yet clear, and each material may yet find its niche. But overall prospects for superconductors impacting the power grid have never been brighter.

3 Superconductor Rotating Machines

3.1 Test Experience with Large Superconductor Rotating Machines

3.1.1 5 MVA, 230 RPM Ship Propulsion Motor

HTS ship propulsion motors using HTS air-core synchronous AC motor technology offer a range of benefits and advantages for both naval and commercial shipping applications [3.1-3.5]. These include high power density (reduced size and weight), high efficiency and low structure-borne noise.

HTS motors offer higher power density than is possible with other technologies due to the combination of high air-gap flux density coupled with a high current density air-core stator winding. A typical US Navy ship needs two propulsion motors; each rated in a range above 30 MW, and 120-150 revolutions/min. Such large motors have been built using conventional technology [3.6] but they are 2.5 to 5 times heavier than what is possible with HTS technology. The U.S. Navy's Office of Naval Research (ONR) funded the 5 MW output power, 230 r/min propulsion motor project by AMSC and Alstom (now Converteam) to validate technologies required to design and build larger ship propulsion motors.

The rotor assembly includes field windings operating at 32 K, their support structure, a cooling loop, cryostat, and electromagnetic (EM) shield shown in Fig. 3.1. An external cryocooler module (also shown) for cooling the field winding is located at the non-driven end of the shaft. The stator assembly includes an AC stator winding, back iron, stator winding support structure, bearing and housing as shown in Fig. 3.2. The motor's characteristic parameters are summarized in Table 3.1 and these parameters were verified with factory no-load and load testing at ALSTOM, Rugby, U.K. as shown in Fig. 3.3. The motor was delivered to U.S. Navy in July 2003.

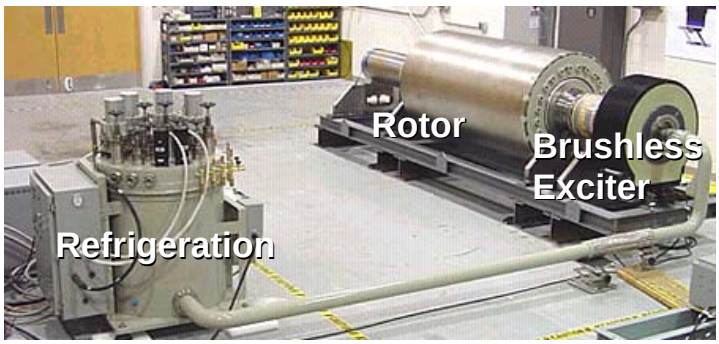

Fig. 3.1: 5 MW HTS rotor assembly undergoing factory testing

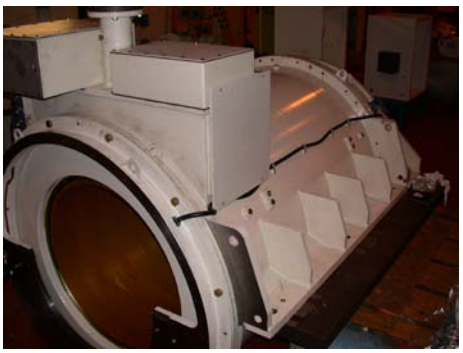

Fig. 3.2: 5 MW built stator

The motor was shipped to the Center for Advanced Power Systems (CAPS) on the campus of Florida State University and coupled with two GE dynamometers. The purpose of the testing was two fold: 1) demonstrate full load performance and 2) perform dynamic stability studies simulating high sea states; see ref. [3.6] for more detailed information. A full load heat run was completed on September 19, 2004 demonstrating >5 MW at 230 rpm until the stator attained steady state temperature. This test was repeated for > 20 hours as an endurance test. Fabrication and testing of the 5 MW motor successfully demonstrated the technology required for this and larger machines including the 36.5 MW discussed in the next section.

Table 3.1: Parameters for the 5 MW HTS motor

Parameter	Value	Units
Nominal rating	5	MW
Rated phase voltage	2400	V (rms)
Rated phase current	715	A (rms)
Power factor at rated load	1	
Rated speed	230	r/min
Frequency at rated speed	11.5	Hz
D-axis synchronous reactance	0.32	pu
D-axis transient reactance	0.24	pu
D-axis sub-transient reactance	0.16	pu

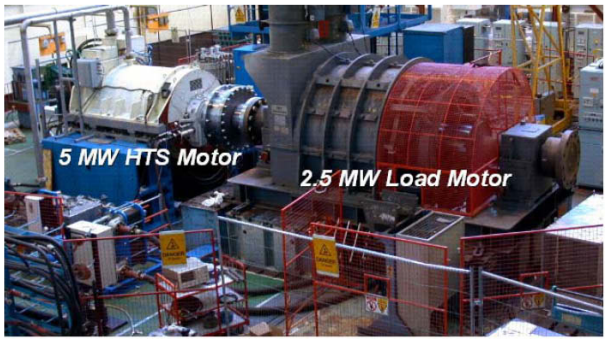

Fig. 3.3 MW, 230 r/min HTS motor coupled with a 2.5 MW load motor

3.1.2 36 MVA, 120 RPM Ship Propulsion Motor

Subsequent to the 5 MW motor program, the Office of Naval Research funded a full scale advanced technology demonstrator. The 36.5 MW High Temperature Superconductor (HTS) motor was designed for navy combatant ship propulsion requiring high performance and power density. With an output shaft speed of 120 rpm, it was designed to generate over 2.9 million Newton-meters (2.2 million ft-lbs) of torque. The design drivers included low system weight with a specific target of 75 metric tons. Other drivers were improved efficiency and shock capability [3.7, 3.8]. This motor represents a 14:1 increase in torque over the 230 rpm, 5 MW HTS motor previously built and tested.

This 36.5 MW HTS motor was designed and built by a team led by American Superconductor (AMSC) as prime contractor and Northrop Grumman, Electronic Systems - Marine Systems (NGES-MS) as lead for the mechanical design. Other team members included Electric Machinery, Inc., BMT-Syntek, Northrop Grumman Ship Systems and Florida State University Center for Advanced Power Systems.

The complete motor system consists of the approximately 70 metric ton motor itself and four ancillary subsystems. The ancillary subsystems consist of three skids (lube oil, stator cooling and rotor refrigeration) and a system controller. The stator is a nine-phase design with insulation rated for 9 kV line to line. This technology demonstrator is designed to operate with three commercial 14 MW variable speed drives (VSD) providing approximately 6 kV line-to-line and 1275 amps. Total system motor and ancillaries shown in Fig. 3.4 weighed less than the 75 metric tons.

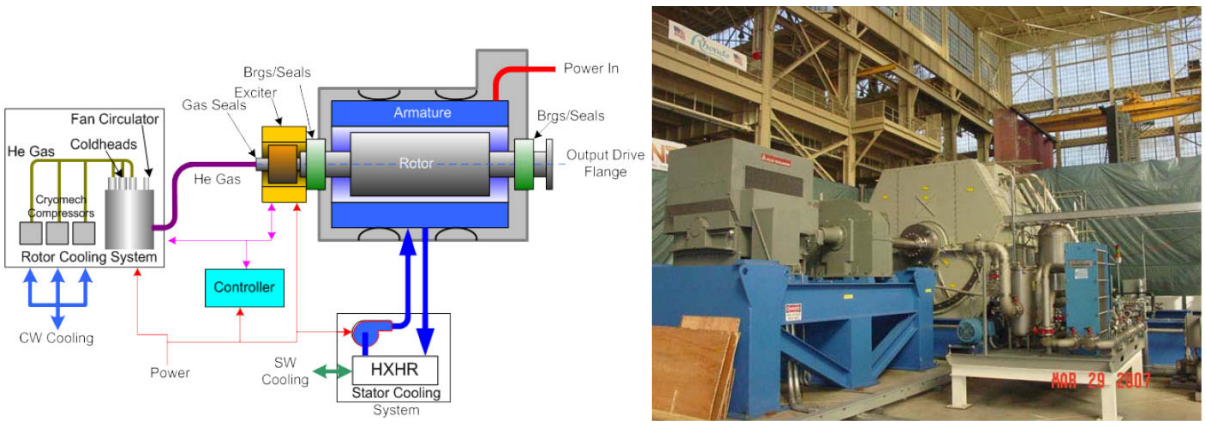

Fig. 3.4: HTS Motor System conceptual drawing and picture from no-load test facility in Philadelphia.

At the heart of this power-dense technology lies a rotor (Fig. 3.5) constructed with first generation HTS wire which permits generation of much higher magnetic fields than is practical with conventional copper windings or possible with present permanent magnet technology. The rotor refrigeration system maintains the HTS field coils at their operating temperature (approximately 30K) with gaseous helium loops to extract heat from the HTS coils.

To best take advantage of this very high rotor flux, the teeth holding the stator windings are non-magnetic. Magnetic teeth would be limited in field by saturation. Completing the technology features of this power dense application, the stator is liquid cooled with dielectric insulating oil.

The factory acceptance tests were performed on the HTS motor in accordance with IEEE Std 115-1995. The motor's design characteristics were fully achieved or exceeded as shown in Table 3.2. Rotating tests verified: mechanical design at 120% over-speed, stator voltage at 110% of rated, stator current at 100% of rated and stator cooling at 100% stator current.

Fig. 3.5: Rotor and rotor cooling system during factory testing prior to shipment to Philadelphia

Table 3.2 Key HTS motor parameters verified

Parameter	Design	Measured
Design Power	37.2 MW	Voltage/ Current >37.2 MW
Voltage	5.8 kV	6.6 kV
Current	1.275 kA	1.28 kA
Stator Winding Temperature	Class F to meet Class B	80.5 C (based on resistance and scaled to 40C inlet)
Efficiency	97%	97%

Full load testing using a water break as a load was completed in Dec. 2008 at the US Navy's land-based test site (LBTS) in Philadelphia PA. In a four-hour heat run, power over 36.5 MW was demonstrated at 127 rpm with 2.3 million N-m of torque. Temperature sensors throughout the stator confirmed temperature stability.

The design, development and manufacture of this large direct-drive ship propulsion motor have been validated by the results of this successful factory and full load testing. All key design predictions were confirmed; the ability to withstand excess voltage and rated current without problem establishes the readiness of this full-scale demonstrator motor for ship propulsion application and is a major benchmark for the credibility of HTS rotating machine technology.

3.1.3 4 MVA, 3600 RPM Ship Generator

Starting in 2002, Siemens in Germany designed and manufactured its second HTS synchronous machine. This machine is designed as a generator for marine vehicle applications rated 4 MVA at 60 Hz and 3600 rpm [3.9]. Consequently, it was tested according to the particular standards for marine vehicle applications of the

"Germanischer Lloyd". Fig. 3.6 shows the machine in the company's test facility in Nuremberg, Germany. The first-ever synchronization of an HTS generator onto the grid was carried out in the mid of June 2005.

The rotor of the machine consists of HTS pancake coils manufactured from Bi 2223-tape from what is now Bruker HTS. The armature winding is an air-gap winding using fully transposed and insulated small diameter strands. It is fixed to the stator core with non-magnetic fibre reinforced plastic (FRP) elements. The armature winding is air cooled [3.10].

As one of the first tests, the open circuit as well as the short circuit characteristic of the machine were measured [3.11]. The results are depicted in Fig. 3.7.

Fig. 3.6: 4 MVA HTS machine

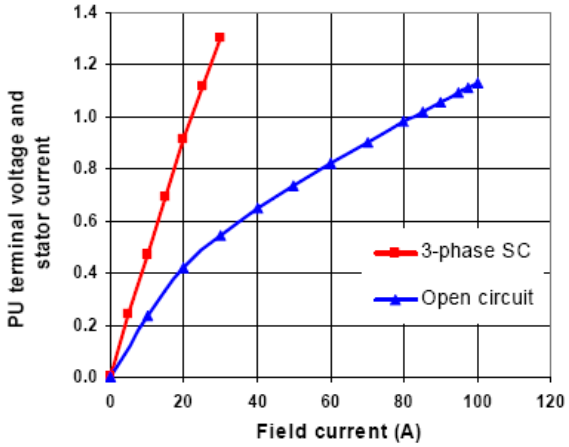

Fig. 3.7: Open circuit and short circuit characteristics of the 4 MVA HTS machine

Furthermore, the efficiency of the machine was measured. A value of 98.7 % was obtained which is approximately 2 % higher compared to a conventional machine of the same rating [3.12]. The detailed relation of partial losses contributing to the overall losses of the machine is shown in Fig. 3.8 [3.13]. Other results are that noise and vibrations of the machine are very low. Operation with underexcitation (cos φ=0) is possible without restrictions. Table 3.3 shows some more selected parameters of

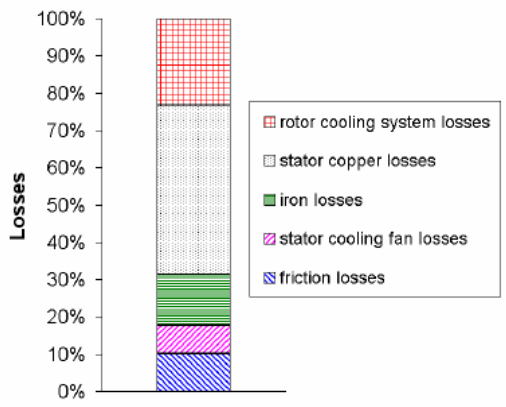

Fig. 3.8: Fractions of losses of the 4 MVA HTS machine

Table 3.3 Technical data of the 4 MVA HTS machine

Rated Power	4 MVA
Rated Voltage	6600 V
Rated Frequency	60 Hz
Rated Speed	3600 rpm
Rated Torque	10.6 kNm
Efficiency at rated load	98.7 %
D-axis Synchronous reactance	0.41 p.u.
Initial short circuit current/nominal current ratio	16
Two pole short circuit torque/nominal torque ratio	7
Steady short circuit current/nominal current ratio	4
Length x Width x Height (cooling system included)	3.3m x 1.9m x 1.8m
Weight	7 to

the machine (measured) [3.14, 3.15]. Starting a new long-term test programm in 2008, the 4 MVA Generator is now operating as a synchronous condenser in the 20 kV distribution network in Nuremberg, Germany. In this application, the machine balances the demand for reative power of mostly inductive consumers at the Siemens Industry Large Drives System Test Center. On average, about 40 MVArh are compensated per day [3.26]. In spring 2009, Siemens announced that the machine had operated successfully over one year.

3.1.4 8 MVA Synchronous Condenser

In a collaborative project between American Superconductor and Tennessee Valley Authority in the US, an 8 MVAR 13.8 kV HTS dynamic synchronous condenser was designed, built and tested for a year in the TVA grid [3.16]. The unit was installed near an arc furnace of the Hoeganaes steel plant in Gallatin, Tennessee, in the United States. It began grid operation on October 10, 2004, was brought into regular operation in January 2005 and operated until November 2005. The equipment was operated to help reduce voltage flicker caused by the arc furnace.

The dynamic synchronous condenser is a generator without a primary power source, and as such it can provide primarily reactive (out-of-phase) power, although a smaller amount of real power can come from the inertia of the rotor. The reactive power is inductive or capacitive depending on whether the grid voltage is greater or less than the voltage induced in the stator coils by the rotating field from the rotor coils. Thus, the synchronous condenser injects capacitive reactive power to compensate for dips in voltage caused by disturbances in the grid. Its response is quasi-instantaneous or subcycle. In this 4-pole machine, the rotor poles were racetrack-shaped coils based on the first generation (1G) HTS wire using the BSCCO-2223 superconductor manufactured by AMSC. Cooling was provided by two Gifford-McMahon cryocoolers and a neon thermosyphon system. A picture of the 8 MVAR machine, in its trailerized unit, is shown in Fig. 3.9.

Fig. 3.9: 8 MVAR dynamic synchronous condenser for TVA test site

The advantages of an HTS-based synchronous condenser, as compared to conventional copper-based machines (which are still used on some grids around the world) are several-fold: Because of the high fields generated by the compact HTS coils, the size and weight of an HTS machine can be less than a comparably rated conventional machine. The machine has a low synchronous reactance, of order 0.5 per unit, as compared to conventional machines, and this enables attaining 100% of

full rating, both capacitive and inductive, with relatively small current excursions in the rotor. The elimination of temperature excursions in the superconducting rotor coils eliminates the thermal fatigue which afflicts conventional machines.

With its capabilities for rapid response in reactive power, the synchronous condenser can be used for flicker mitigation; this was the application for the 8 MVAR unit at Hoeganaes. It can also be used for grid stabilization, power quality, low-voltage ride-through in wind farms, or long-term reactive compensation, since it works effectively on all timescales. It can operate in a purely rapid-response mode to grid variations, or it can be designed for automatic voltage regulation by adjustment of rotor current through a brushless exciter, on a time scale of seconds.

At the Hoeganaes site, transient disturbances occurred during ½ to 1 hour melt cycles in the arc furnace at 1 hour intervals. Rapid disturbances occurred, often at one-second intervals. The machine absorbed transient disturbances with very high negative (>50%) and zero sequence (>20%) current components; the magnetic fields created by these sequences were absorbed effectively in a continuous damper winding in the form of a copper shell around the rotor. The stator winding stayed well below the peak allowable temperature. Even with only 8 MVAR rated capability in the synchronous condenser as compared to a power load of 45 MVA for the arc furnace, voltage disturbances dropped from an average of 1.3 kV to 0.8 kV with the unit on-line. Interestingly, there was also a beneficial effect on the Gallatin generating station which provided power to the Hoeganaes site: The variance in voltage disturbance dropped from an average of 0.055 kV to 0.035 kV with the unit on-line. With active changes in reactance during each melt cycle, the unit experienced an enormous number of reactive events – of order 5 million – during the year. While certain peripheral equipment required maintenance during this period, the rotating machine itself performed very successfully in what must be considered one of the most rigorous in-site tests of HTS equipment to date.

Because of the successful operation of this first unit, two additional commercial HTS synchronous condensers with 12 MVA ratings were initially ordered by TVA. However, a joint decision was made by TVA and AMSC to cancel this order, and AMSC has put its SuperVAR® synchronous condenser product on hold. A principal issue is rising materials costs which have made the technology less competitive compared to power electronic systems providing some of the same reactive compensation functions. Significantly higher ratings (≥50 MVAR) were also identified as the main market need, requiring a new round of larger machine development and demonstration. As HTS wire costs and cryogenic costs come down, and with optimized design for manufacturing, the HTS dynamic synchronous condenser could eventually be re-established as a viable commercial product.

3.2 State-of-the-Art of Superconductor Rotating Machine Development

Worldwide, researchers and engineers are engaged in developing superconductor machines using different design topologies. From a basic standpoint, the use of bulk HTS could be considered as well as HTS tape together with magnetic material such as iron and permanent magnet components. Since the advantage of superconductivity with its refrigeration requirements is limited in smaller sizes, manufacturers focus primarily on MW-rated machines with coil-based windings made from commercially available HTS tape. As the HTS tapes are sensitive to AC fields and AC currents, their use in electrical machines is economically most attractive in DC windings, for example in rotor field windings of synchronous machines.

Up to now, most HTS machine demonstrators employed 1G HTS wire (Bi-2223). However, a high penetration or even complete replacement by 2G HTS wire (YBCO coated conductor) is likely because this material becomes now commercially available in long length and promises a substantial decrease in wire prices with equal or increased electrical performance and equivalent or even better mechanical properties.

Most of the teams concerned with design of superconducting machines deal with radial flux type synchronous machines. The principle design of these machines is given by a three-phase copper winding in the stator and a HTS field winding in the rotor. Several concepts are available for application to different radial flux type machines. The options for HTS machines can be differentiated by the design concepts of rotor and stator components, and electrical/mechanical and cooling concepts in both fields. Regarding the rotor, there are machines with and without magnetic rotor iron core. The stator designs differ by the use of magnetic or non-magnetic stator teeth. Advantages and disadvantages of either design concept are explained and evaluated in [3.17] and [3.18].

The latest developments are successful factory and full-load tests of a 36.5 MW HTS motor for ship propulsion by American Superconductor Corp. in collaboration with Northrop-Grumman [3.18] which followed an earlier successful 5 MW demonstration [3.3], [3.6] in collaboration with Alstom (now Converteam), a 1 MW HTS motor by KERI and Doosan Heavy Industries developed under the Korean DAPAS program [3.20], and a 4 MVA HTS generator by Siemens [3.10]. While the development of a utility 100 MVA HTS rotor by General Electric [3.21] was suspended, other groups continue with the development of radial flux type HTS machines primarily in the field of ship propulsion but also hydro and wind power generation [3.18], [3.22]. Zenergy Power and Converteam have announced a project to build a 1.25 MW hydrogenerator. Another significant development is the recognition that compact, light-weight HTS generators can enable 10 MW-class generators for off-shore wind turbines. Three technology development programs towards this goal have been launched by Converteam, American Superconductor in collaboration with TECO-Westinghouse, and by the Danish Technical University in collaboration with Riso National Laboratory in Denmark.

As described in a previous section, the only rotating machine so far tested in an in-grid utility environment is American Superconductor's 8 MVAR SuperVAR machine, a dynamic synchronous condenser, which successfully experienced and reactively-compensated of order 5 million voltage sag events caused by an arc furnace in a nearby steel plant in the Tennessee Valley Authority grid [3.16]. The Siemens 4 MVA Generator, which was synchronised and tested as a generator in 2005, is now operating as a synchronous condenser, continuously balancing the Siemens Industry Large Drive Test Center's demand for reactive power, thus compensating on average about 40 MVArh each day [3.26].

In addition to radial flux type HTS machines two other concepts are under exploration. A Japanese team including Sumitomo Electric and IHI finished the development of a 365 kW axial flux type HTS motor which is cooled by liquid nitrogen [3.23], [3.24]. Another design concept is used for a development carried out by General Electric for a 5 MW high rotational speed generator for the US Air Force. Here, a homopolar design concept is utilized having a stationary HTS winding that excites the rotor iron of the machine [3.25]. The Korean based KERI and Doosan Heavy Industries have also announced plans to explore this concept [3.20].

An overview about finished or running HTS machine developments covering the MW range is given in Table 3.4. The table reflects no ranking and may not be complete since a lot of R&D is going on world-wide. It can be expected, that within the next decade first commercial applications will be in the market.

Table 3.4 Recent and current HTS machine developments

Manufacturer	**Machine**	**Timeline**
AMSC (US)	5 MW demo-motor	2004
	8 MVA, 12 MVA synchronous condenser	2005/2006
	40 MVA generator design study	2006
	36 MW ship propulsion motor 8 MW wind generator design study	2008 2010
GE (US)	100 MVA utility generator	2006 (discontinued.)
	5 MVA homopolar induction motor	2008
LEI (US)	5 MVA high speed generator	2006
Reliance Electric (US)	10.5 MVA generator design study	2008
IHI Marine, SEI (JP)	365 kW ship propeller motor	2007
	2.5MW ship propeller motor	2010
Doosan, KERI (Korea)	1 MVA demo-generator	2007
	5 MW motor (homopolar)	2010
Siemens (Germany)	400 kW demo-motor	2001
	4 MVA industrial generator	2005
	4 MW ship propeller motor	2009
Converteam (UK)	200 kW demonstrator	2006
	1.25 MVA hydro-generator	2008
	500 kW demo-generator	2008
	8 MW wind generator design study	2010

4 Superconducting Cable

Superconducting power cable projects utilizing High-Temperature Superconductors (HTS) have been undertaken since the late 1990s. A summary of recent, actual and future HTS cable projects is given in Table 4.1. All these projects are directed to underground cables; HTS does not compete for overhead lines, although some creative new concepts have been proposed at Los Alamos National Laboratory in the US.

Table 4.1: HTS cable projects

Manufacturer	**Place/Country/Year** [1)]	**Type**	**Data**	**Supercond.**
Furukawa	Yokosuka, JP, 2004	CD	77 kV, 1 kA, 500 m, 1-ph.	BSCCO
Innost	Yunnan, CN, 2004	WD	35 kV, 2 kA, 33 m, 3-ph.	BSCCO
Sumitomo	Albany, US, 2006	CD	34.5 kV, 800 A, 350 m, 3-ph.	BSCCO
Ultera	Columbus, US, 2006	Triax	13.2 kV, 3 kA, 200 m, 3-ph.	BSCCO
Sumitomo	Gochang, KR, 2006	CD	22.9 kV, 1.25 kA, 100 m, 3-ph.	BSCCO
LS Cable	Gochang, KR, 2007	CD	22.9 kV, 1.26 kA, 100 m, 3-ph.	BSCCO
Sumitomo	Albany, US, 2007	CD	34.5 kV, 800 A, 30 m, 3-ph.	YBCO
Nexans	Hannover, D, 2007	CD	138 kV, 1.8 kA, 30 m, 1-ph.	YBCO
Nexans	Long Island, US, 2008	CD	138 kV, 1.8 kA, 600 m, 3-ph.	BSCCO
Ultera	New York, US, 2010	Triax	13.8 kV, 4 kA, 240 m, 3-ph.	YBCO
Ultera	New Orleans, US, 2011	Triax	13.8 kV, 2.5 kA, 1700 m, 3-ph.	-
Ultera	Amsterdam, NL, -	Triax	50 kV, 2.9 kA, 6000 m, 3-ph.	-
Nexans	Long Island, US, -	CD	138 kV, 2.4 kA, 600 m, 1-ph.	YBCO
LS Cable	Gochang, KR, 2011	CD	154 kV, 1 GVA, 100 m, 3	-
LS Cable	Seoul, KR	CD	22.9 kV, 50 MVA, 500 m, 3	YBCO
Sumitomo	Yokohama, JP, 2013	CD	66 kV, 200 MVA, 200	BSCCO
Sumitomo	TEPCO, JP	CD	66 kV, 5 kA	-
Furukawa	TEPCO, JP	CD	275 kV, 3 kA	BSCCO
Sumitomo	Chubu U., JP, 2010	CD	10 kV, 3 kA DC, 20 m, 200 m	BSCCO
VNIIKP	Moscow, RU	CD	20 kV, 30 m and 100 m	YBCO
Nexans	Spain	CD	10 kV, 30 m	BSCCO

1) year of energization

There are two basic different dielectric designs of HTS cable: 'warm dielectric' (WD) and 'cold dielectric' (CD). In a 'warm dielectric' cable, only the superconductor phase layers are cooled by liquid nitrogen, while the cable insulation (the dielectric) and the normal-conducting screen layers are at ambient temperature (Fig. 4.1). This relatively simple design provides high power density while minimizing the number of HTS wires required for a given transmitted power. Drawbacks compared to cold-dielectric designs (Fig. 4.2) are higher electrical losses, translating into additional cooling stations, higher inductance and phase spacing in order to limit the adverse effect of the stray electromagnetic fields (EMF) generated by the other phases on the current transport capacity of an individual phase.

HTS cables also differ according to the phase architecture. In the recently energized transmission voltage LIPA cable, Nexans demonstrated a CD design with a separate cable containing HTS phase conductor and coaxial HTS shield for each phase. Ultera (Southwire/nkt Cables joint venture) has demonstrated a CD design called Triax^{TM} for distribution-level applications with all three phases wound concentrically in one cable. This design requires no HTS shield layer, and external EMF is largely compensated. Sumitomo Electric has demonstrated a three-core design in which the three phases, each surrounded by its HTS shield, are positioned within one cryostat and cable. An earlier WD design by Pirelli (now Prysmian) at Detroit Edison used a separate cable for each phase.

Two major technical challenges in the production of an HTS power cable are the high-voltage terminations and the thermal contraction of the cable core. Compared to conventional terminations, HTS cable terminations, in addition to being at high voltage, have to bridge the temperature range from ambient to 77 K. Several successfully operating high-voltage terminations (up to the 161 kV level demonstrated by Nexans in the LIPA project) show that this technical challenge has been mastered.

The thermal contraction management has been addressed and solved for lengths up to several hundred meters in several ways. In SEI's design, the three cores are wound in such a way that each phase has the possibility to move inside the cryostat, and to redistribute this degree of freedom all along the cable's length. In Nexans' design in the LIPA cable, the cable can slide at each termination.

HTS cables offer a variety of advantages compared to conventional cables, among them:

- Higher current and power capacity at the same voltage level and cross-section
- Ease of installation amid dense underground infrastructure
- Lower impedance

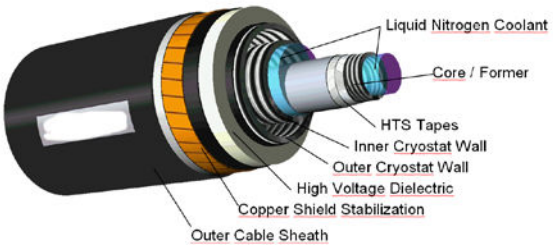

Fig. 4.1: Warm dielectric cable

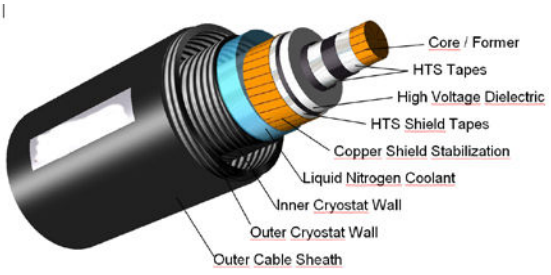

Fig. 4.2 Cold dielectric cable

- No external electromagnetic fields (cold dielectric cables)
- Thermal independence from surrounding area
- Increased efficiency of operation
- Option of current limiting functionality

Per unit length, HTS cables will likely continue to be more expensive than conventional cables rated at the same power. The economic impact of HTS cables has to be evaluated from a system perspective. As an example, HTS cable systems allow a higher power throughput at a given operating voltage, so that a costly system voltage upgrade can be avoided. By adding a parallel HTS link to an existing conventional cable link, the transport capacity of the line can be dramatically increased without increasing the fault current when the current limiting functionality of the HTS cable is exploited. Then the lifetime of the existing conventional links can be increased. The ability to use existing right-of-ways instead of having to acquire and permit new ones is another important benefit.

4.1 Field Test Experience with Superconductor Cables

4.1.1 77 kV, 1 kA, 500 m, Super-ACE and other Cable Tests in Japan

In a project of Sumitomo Electric (SEI) with TEPCO, a 100 m long 66 kV, 115 MVA cold-dielectric three-core cable was designed, fabricated and successfully tested in 2002 at the CRIEPI (Central Research Institute of Electric Power Industry) test laboratory in Yokosuka, Japan. This cable used SEI 1G HTS wire.

In a project called Super-ACE with Furukawa, CRIEPI and Super-GM at the CRIEPI site in Yokosuka, Japan, a single-core, 500 m, 77 kV, 1 kA cold dielectric cable was designed, fabricated and tested in 2004-5 [4.1]-[4.3]. The cable structure is shown in Fig. 4.3. Furukawa 1G HTS wire was used. The 500 m long loop was set up to simulate real life conditions. It included two U-bends with 5 m radius and a section that was raised 10 m. The layout and the cooling system are shown in Fig. 4.4. In the test, critical currents (Ic) of HTS conductor and HTS shield at 73 K were 1910 A and 1620 A respectively, with heat leak of 1.21 W/m, and a pressure drop of 100 Pa/m at an LN_2 flow rate of 50 L/min. Rated loading tests corresponding to degradation of the insulation over 30 years were carried out, and there was no degradation in the cable. Moreover, overload and limiting tests were successfully performed under the adverse conditions of over-voltage, over-current and stopping of refrigerators and pumps. A new project is underway for an in-grid demonstration cable by SEI and TEPCO, using SEI 1G HTS wire. A short cable using 2G HTS wire was jointly fabricated and tested by SEI and Furukawa, and a new project supported by NEDO in Japan will further develop low loss 66kV and high voltage 275kV HTS cables based on 2G HTS wire.

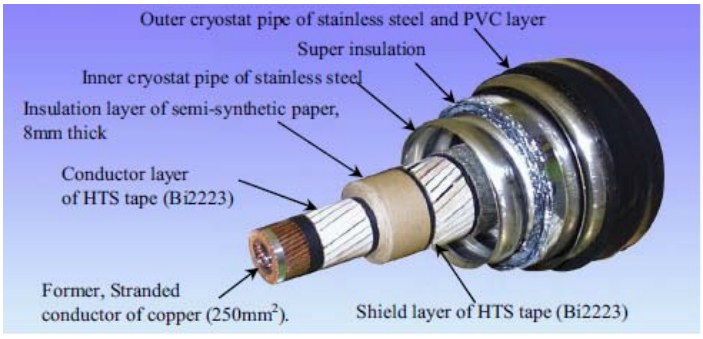

Fig. 4.3: Structure of 500m HTS cable

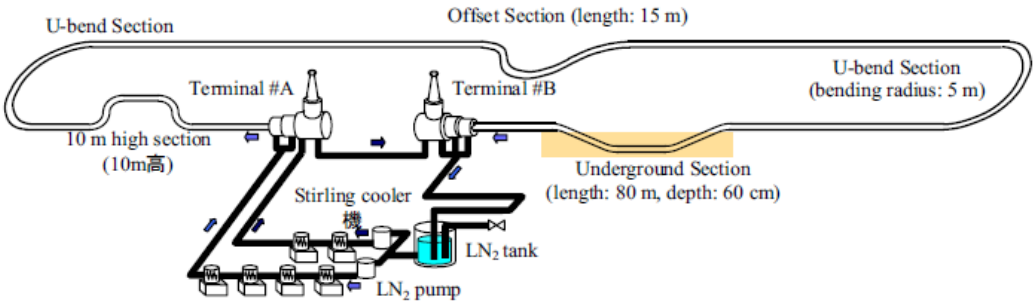

Fig. 4.4: Layout of 500m HTS cable and the cooling system

4.1.2 138 kV, 2.4 kA, 660 m Cable , Long Island Power Authority

The 600 m long, Long Island Power Authority Cable Project is the longest and highest voltage HTS cable project undertaken to date [4.4]. At a voltage level of 138 kV and a rated current of 2.4 kA, the cable has a nominal transmission capacity of 574 MVA. Voltage level, rated current and transmission capacity are also the highest in any HTS power cable so far. Pictures of the cable termination and the cable transport are shown in Fig. 4.5 and Fig. 4.6. A particularly important feature of this cable system is that it was designed to full utility requirements so as to remain a permanent operating element of the LIPA grid.

The project partners are American Superconductor (AMSC), Nexans, Air Liquide, and the Long Island Power Authority (LIPA), and the project was partially supported by the US Dept. of Energy (DOE). The cable utilizes AMSC 1G HTS (Bi-2223) tapes in a cold dielectric design with two phase layers. It has been installed in a LIPA right of way in Holbrook, NY, and was successfully commissioned in April 2008. It is operating in the LIPA grid and is the first HTS system operating in a live grid at transmission level voltage. A follow-on partially-USDOE-supported project is underway with the same partners, called LIPA-2, in which one of the three phases will be replaced by a cable using AMSC's 2G YBCO wire.

Fig. 4.5: 138 kV HTS cable with terminations

Fig. 4.6: 600 m HTS cable with evacuated cryogenic envelope on one drum

4.1.3 34.5 kV, 0.8 kA, 350 m Cable, Albany

This distribution-voltage in-grid cable was a co-operation between SuperPower, Sumitomo Electric Industries, BOC, and National Grid (Fig. 4.7), and partially supported by USDOE and the New York State agency NYSERDA. The 350 m long HTS cable installed in Albany was made up of two sections of 320 m and 30 m of length, respectively. Between the two sections, it features the world's first in-grid demonstration of an HTS cable splice. This cable commenced operation in the grid of National Grid since July of 2006 [4.5]. In the original installation both sections of the cable used 1G HTS wire (Bi-2223 material); a follow-on project replaced the 30 m long section of the cable with a 30 m section made from 2G HTS wire (YBCO) from

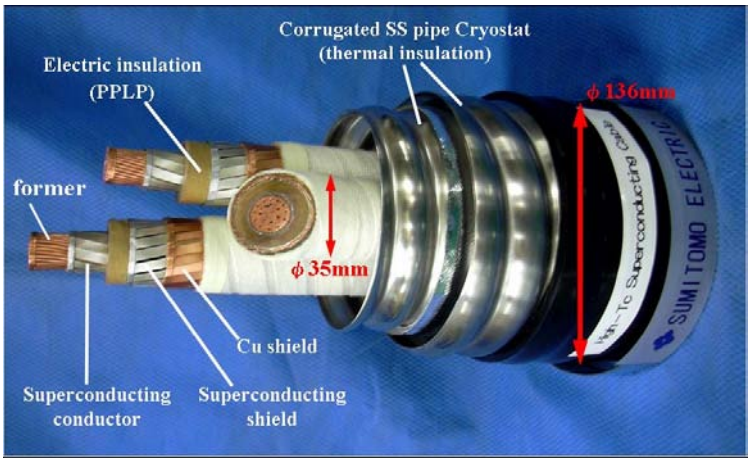

Fig. 4.7: 3 in one HTS cable

SuperPower. The successful commissioning took place in early 2008 and in-grid operation was successfully completed in spring 2008. Multiple faults have been successfully handled.

4.1.4 13.2 kV, 3 kA, 200 m, Columbus

The Columbus cable project follows on two successful in-grid projects, one by Southwire providing power to its Carrollton manufacturing facility in Georgia US (30 m, 12.7 kV, 24 MVA), which ran for over 5 years, and another by nkt Cables in Copenhagen (30 m, 30 kV, 104 MVA), which also served customers for over a year. The Columbus project was a collaboration between Ultera Cables (a joint venture formed by nkt Cables and Southwire), Oak Ridge National Laboratory, Praxair, American Superconductor, and American Electric Power [4.6], and was partially supported by USDOE. The design of this cable installed in the Bixby substation in Columbus, OH, is significantly different from the three cables described above, even though the dielectric is immersed in liquid nitrogen and the cable is thus of a 'cold dielectric' design. In the triaxial design as shown in Fig. 4.8, all three phases are wound concentrically onto one cable core. The triaxial design significantly reduces the number of HTS tapes needed by eliminating the need for a HTS shield, and is generally more compact and power-dense than three separate cables for each phase. The termination of the Triax cable is shown in Fig. 4.9. As it also requires only one cable cryostat, additional cost savings may be realized.

This 300 m, 14.5 kV, 63 MVA cable with 1G HTS wire continues to run since its energization in 2006 and has successfully handled several faults.

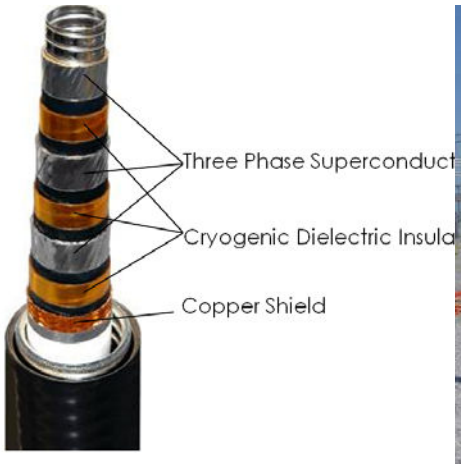

Fig. 4.8: Triax cable

Fig. 4.9: Termination of Triax cable

4.1.5 35 kV, 2 kA, 30 m Cable, Yunnan

A 30 m, 35 kV / 2 kA, 3-phase cable by Innopower Superconductor Cable Co., with 1G HTS wire from InnoST, has been put into operation at Puji substation in Kunming, Yunnan Province, China [4.7]. Collaborators include the Yunnan Electric Power Group, the Institute of Plasma Physics of Academia Sinica, Research Institute of China Electronics Technology Corporation, Shanghai Cable Works, Tsinghua and Huazhong Universities and Nexans. This is the only recent cable project utilizing the warm dielectric design; the project was supported by the Chinese Ministry of Science and Technology (MOST). This cable continues in operation since April 19, 2004, now the longest continually running HTS cable. It has had no major faults or break downs, and has demonstrated satisfactory performance according to all design parameters. Nexans supplied the outer cryogenic envelope with XLPE-insulation. Another cable was developed by the Institute of Electric Engineering of the Chinese Academy of Sciences in collaboration with ChangTong Cable Company and also supported by MOST. It has been installed to provide power to the ChangTong cable manufacturing facility in Baiyin, China; it ran successfully beginning in 2005 and has now been decommissioned.

4.1.6 22.9 kV, 1.26 kA, 100 m Cable, Gochang

Supported by the South Korean DAPAS program (Development of Advanced Power system Applied by Superconductivity technologies), LS Cable and KERI have demonstrated a 30 m 22.9 kV, 50 MVA HTS cable. This has been followed up by a 100 m 22.9 kV, 1200 A demonstration, using AMSC 1G wire, at the Gochang test site of KEPCO. This 3-phase cable was set up to simulate real conditions. It included a joint box, an U-bend on the ground, 90 degree bended pipe duct and an underground tunnel. A picture of the cable termination is shown in Fig. 4.10.

Sumitomo Electric and KEPRI are now also demonstrating a 100 m, 22.9 kV 50 MVA HTS cable using Sumitomo Electric's 1G HTS wire, at the Gochang test site. As a next step, the DAPAS program is targeting a 154 kV test cable, and LS Cable and

Fig. 4.10: 22.9 kV HTS cable with termination (3 phase in 1 termination)

KEPCO are building a 500 m 22.9 kV 50 MVA cable for in-grid installation in Seoul.

4.1.7 2G-HTS-based Cables

In addition to the in-grid demonstation of a 2G HTS cable section at the Albany site described above, several cable projects have started to demonstrate feasibility of 2G HTS wire for this application. Together with American Superconductor, Nexans has successfully manufactured and laboratory-tested a one-phase 30 m, 138 kV cable with a transmission capacity of 435 MVA. In a project sponsored by the USDOE, AMSC, Nexans, Air Liquide and LIPA will also be upgrading one of the phases of the 600m LIPA transmission cable into a 2G-wire-based cable.

In Europe, Super3C was a now completed project supported by the European commission which successfully demonstrated a 30m, 10 kV, 1 kA 2G HTS cable. The European partners are Nexans, Bruker HTS, E.ON Energie, E.ON Engineering, Center for Functional Materials ZFW – Göttingen (Germany), Barcelona Institute of Materials Sciences (CSIC) and Labein (Spain), Tampere University of Technology (Finland), Air Liquide (France) and Bratislava Institute of Electrical Engineering (Slovakia).

Another significant development is the project of American Superconductor, with its cable partners Southwire and Ultera joint venture partner nkt Cables, to develop a new fault current limiting cable as part of a U.S. Department of Homeland Security (DHS) initiative to protect the nation's power systems. The project is in collaboration with Con Edison of New York City. The goal is to demonstrate a cable which can enable a more reliable and secure power system, through the "Secure Super Grids^{TM}" concept. The first demonstration, targeted for 2010, will be a several hundred meter long cable with a voltage level 13.8 kV, rated current 4 kA and a transmission capacity of 96 MVA. This will allow linking NYC substations at the distribution level, providing alternative power links to a given area in case of a disturbance in any one of the linked substations.

A key element of this project is to introduce current limiting functionality directly into the cable through the use of second generation HTS wire with relatively high resistance in its non-superconducting state. The goal is to enable the distribution-level connections between substations without increasing the NYC grid's overall fault current, which is already high and nearing breaker ratings. The fault current limiting cable uses the fact that resistance increases rapidly as current exceeds the critical current; the resulting impedance reduces the magnitude of the fault current. A key design issue is to avoid allowing the wire temperature to increase during the fault to the point where bubbles appear in the liquid nitrogen, endangering the dielectric integrity. For a situation like NYC where both cable links between substations and fault current control are needed, this fault-current-limiting cable solution is expected to have a substantial advantage as compared to a separate cable plus standalone fault current limiter, because it reduces the required footprint of the installation and significantly lowers cost. In cases where fault current limitation is needed without an additional cable link, a standalone fault current limiter is the appropriate solution.

Another major HTS cable initiative in the US is the USDOE-sponsored project In New Orleans, where Southwire (Ultera) plans together with Entergy to install a 1700 m 13.8 kV cable with a current of 2.5 kA and a capacity of 60 MVA. A major advantage of this installation will be providing increased power to an urban center while avoiding construction of a new substation. As of spring 2009, the wire type for this installation has not yet been finalized; it could be either 1G or 2G. 2G-based cables are also being developed in Japan; 66kV and 275kV. New HTS cable projects are being actively pursued in Amsterdam and Moscow in Europe.

4.2 State-of-the-Art of Superconductor Cable Development

In summary, HTS cables for both distribution and transmission links are one of the most promising grid applications of HTS technology, and utilities around the world are showing increasing interest. Even though HTS cable installations are still expensive, the array of benefits is bringing HTS cables close to commercialization. Extensive testing around the world is demonstrating that all the basic technical challenges have been overcome, and a strong track record of reliability in the demanding grid environment is developing. Current HTS cable projects have progressed to the point where almost all cable systems currently under consideration are of the cold dielectric design, which offers the full range of benefits of HTS cables. Additionally, 1G HTS wire with Bi-2223 is being replaced by 2G HTS wire with YBCO as the conductor of choice for HTS cables, due primarily to its expected lower cost. The use of 2G HTS wire, when configured with a high resistance stabilizer, is also opening a new and potentially very important avenue for HTS cable systems by making them inherently fault current limiting.

One other development of note is the first test of a 20 m single-pole DC cable rated at 10 kV and 3 kA, at Chubu University near Nagoya, Japan, with the cable fabricated by Sumitomo Electric [4.8]. A follow-on 200 m DC cable test is planned by the end of 2009. In contrast to all other HTS cables which are AC, this DC demonstration opens up novel applications, such as high efficiency transmission of renewal power long distances to major population centers. The high efficiency is achieved because AC losses are avoided.

5 Superconducting Fault Current Limiter (SCFCL)

5.1 Field Test Experience with SCFCLs

Up to now, three successful SCFCL field tests took place; however a series of new field tests is starting as of 2009. The first one was performed with a shielded core type SCFCL by ABB (Asea Brown Bovery) in 1996 in Switzerland [5.1]. A second field test with a distribution type SCFCL was performed with a 10 MVA, 10 kV resistive SCFCL using bulk MCP-BSCCO 2212 superconductor [5.2], [5.3]. This test took place from March 2004 until April 2005 in a busbar coupling location in the grid of RWE in Netphen, Germany. A third successful field test started in China in 2005 with a 6 kV, 1.5 kA diode bridge type SCFCL [5.4], [5.5].

This section describes the main test results of SCFCL field tests, shows the recent progress with resistive SCFCLs based on YBCO coated conductors and summarizes the state-of-the-art of SCFCL R&D. In addition, R&D results on superconducting fault current limiting transformers are reported, along with some of the new units starting test.

At present, there are many different types of SCFCLs and it is difficult to forecast which type will be the most promising for the future. An overview about the different types and attractive SCFCL applications is given in [5.6]. Fast and effective current limitation can be achieved with all FCL types. The main differences are with respect to recovery time, fail-safety, normal operation loss and impedance, and size and weight. It is common understanding that the most compact design is offered by the resistive SCFCL whereas fastest recovery is achieved with types not utilizing the quench of the superconductor.

5.1.1 10.5 kV, 70 A Shielded Iron Core Type SCFCL

Ten years after the discovery of high temperature superconductivity in 1986, the first SCFCL field test took place in a power plant in Switzerland in 1996. ABB successfully build and tested a 10.5 kV, 70 A shielded core type SCFCL (see Fig. 5.1). The device was installed in series to the auxiliary transformer of the power plant. In laboratory tests three-phase short-circuits with prospective currents of up to 60 kA were limited to 700 A in the first half wave. After 50 ms the current was further reduced to about 3 times the nominal current. Dielectric tests up to 90 kV BIL and 50 kV AC were

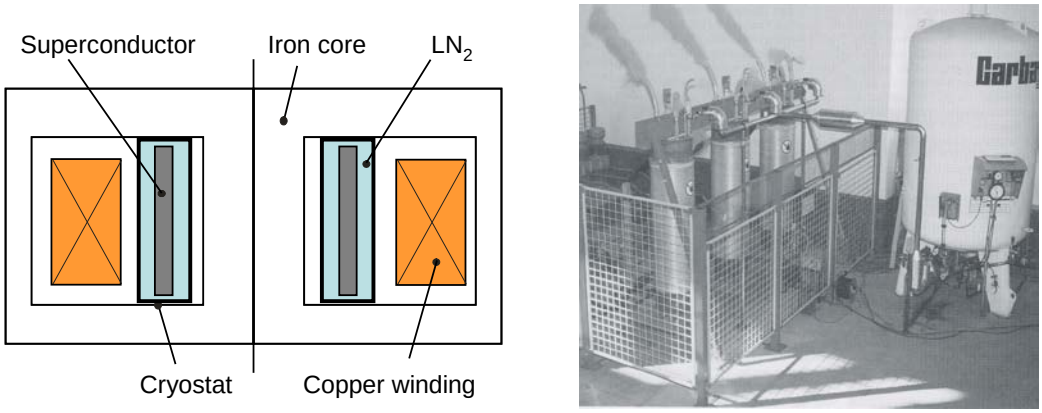

Fig. 5.1 Left – Scheme of shielded core type SCFCL
Right – Picture of shielded core type SCFCL installation [5.1]

performed. During the one year endurance test no short-circuit occurred. For simplicity a LN_2 reservoir was used for cooling instead of a closed cryogenic cooling system. The total loss was 40 Watt at 77 K and consists mainly of the current lead loss and the cryostat loss.

Although this project reached an important milestone with the first superconductor device tested in a power plant under actual operation conditions, R&D on this SCFCL type was discontinued due to the fact that SCFCLs following the shielded core concept would have rather high volume and weight.

5.1.2 10 kV, 600 A Resistive Type SCFCL

A three-phase resistive type 10 kV, 10 MVA SCFCL demonstrator named CURL10 was built in 2003 and successfully tested for one year within the distribution grid of RWE in Germany [5.2], [5.3]. Pictures of CURL10 and the main data are given in Fig. 5.2 and Table 5.1. MCP-BSCCO-2212 bifilar coils, melt-case cylinders machined into a bifilar configuration, from Nexans SuperConductors were used as HTS components [5.7]. A total of 90 HTS components were installed, 30 for each phase.

For a resistive type SCFCL this was the world-wide first field test and it underlined the technical feasibility of this SCFCL type for medium voltage applications. From 2005 to 2007, the CURL10 system passed a further long-term test at Forschungszentrum Karlsruhe.

Field test safety issues

Since SCFCLs are protection devices in power systems their reliability and safe operation is a very important issue. Before, during and after the field test many different tests were performed on the CURL10 system to ensure safety and reliability of the system.

Before the field test the following major tests and items have to be considered mainly to confirm safety and quality issues:

- German TÜV certification for cryostat
- Combined short-circuit and lightning voltage test at sample configuration
- Several short-circuit tests of each HTS

Table 5.1: Main data of CURL10

Voltage	10 kV
Current	600 A
Power (3-ph.)	10 MVA
Max. short-circuit time	60 ms
Max. peak sc. current	8.75 kA
Operating Temperature	66 K
HTS Material	Bi 2212 bulk

Fig. 5.2: 10 kV, 10 MVA resistive SCFCL CURL10.
Left - CURL10 and the cryostat insert
Right - CURL10 during installation

component

- Final quality check of each HTS component before installation
- Separate current and voltage test after assembly of the SCFCL system
- Three-phase short-circuit test of the SCFCL system at a power laboratory
- Separate on-site current and voltage test of the SCFCL system before grid connection

During the field test important safety issues mainly concerning the safety of the SCFCL system and the integration into the grid have to be considered. To ensure a reliable operation the following safety issues were implemented:

- Remote continous monitoring of most important parameters
- Measurement of SCFCL current and switch off if continous current I is larger than I_{max}
- Measurement of cryostat pressure and switch off if pressure p larger than p_{max}
- If the auxiliaries fail then switch off the SCFCL immediately
- Installation of circuit breaker with over current time protection in series with SCFCL

Field test results

The field test was performed from March 2004 until April 2005 in a 10 kV substation in the RWE grid at Netphen near Siegen, Germany. The SCFCL was installed in a busbar coupling location as shown in Fig. 5.3. Within a first test phase a first objective was to ensure a safe and reliable cryogenic operation. In this phase it turned out that the following items needed some improvement:

- Pressure instability occurred after some days of operation. This was solved by making changes in the cryogenic control circuit.
- One sealing needed to be exchanged before normal maintenance.
- The air cooling system needed an improvement to keep the temperature down in the container during hot summer days.

Afterwards the cryogenic system showed a reliable and safe operation. The two refrigerators had a total runtime of 6500 h and 4000 h.

In a next step the demonstration of a continous operation with current flow through

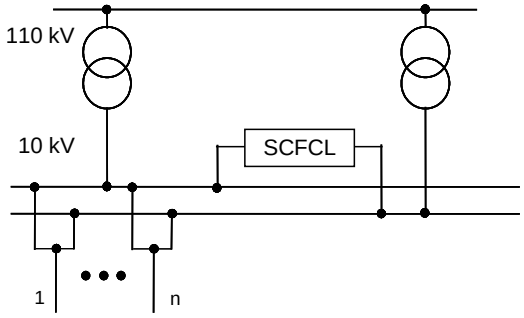

Fig. 5.3: CURL10 installation scheme in busbar coupling location

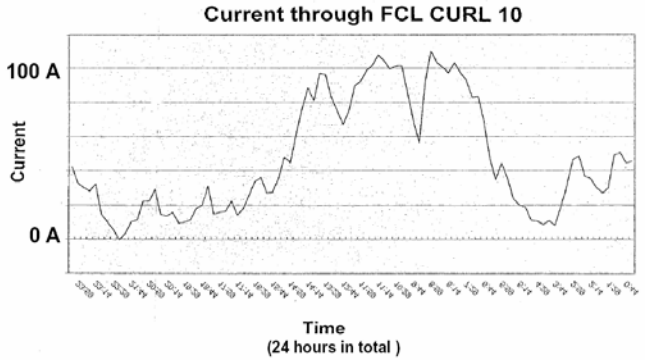

Fig. 5.4: Typical load curve of CURL10 during field test

the SCFCL was the main objective. Figure 5.4 shows a typical day curve of the current. Because of the busbar coupling location of the SCFCL the current is typically much less than the rated current of 600 A. It happened one time during operation that the continous current exceeded the maximum current (at that time the maximum current was adjusted to 200 A) and the SCFCL was shut off as expected.

Unfortunately, no three-phase fault occurred during the field test. In November 2004 a single phase fault occurred. In this 10 kV grid location a single phase fault does not cause a large short-circuit current and consequently no quench occurred in the SCFCL. The grid protection system shut off this single phase fault properly.

In March 2005 the SCFCL was disconnected from the grid and in April the SCFCL was removed from the substation. A comparison of the AC loss measurement before and after the field test showed no change in AC losses. From this result it can be concluded that the connections and the superconducting material showed no degradation during this one year field test.

5.1.3 10.5 kV, 1.5 kA Diode Bridge Type SCFCL

A third SCFCL field test started in August 2005 with a diode bridge type SCFCL [5.8]. A 10.5 kV, 1.5 kA demonstrator (see Fig. 5.5), developed by the Institute of Electrical Engineering of the Chinese Academy of Sciences in Beijing, was installed in a substation located in Hunan, China [5.4] [5.5]. Several successful tests including insulation and short-circuit tests are reported. This SCFCL was the first ever to experience a three phase fault in the grid.

Fig. 5.5: Left – HTS coil for diode bridge type SCFCL
Right – Installation of 10.5 kV, 1.5 kA diode bridge type SCFCL at substation in Hunan, China

In comparison to the original SCFCL diode bridge circuit invented by Boenig [5.9], this demonstrator is without a DC current source and has several IGCTs with a shunt resistance in series connection to the HTS coil. When the current reaches a set value the IGCTs will switch off and the HTS coil and the resistor will limit the current simultaneously. A short recovery time of less than 12 ms is reported, fast enough to allow automatic reclosing of a breaker and return to the normal state.

5.1.4 12 kV & 35 kV DC Biased Iron Core Type

Another type of fault current limiter is called the DC biased iron core type FCL [5.6]. A superconductor coil biases a transformer yoke into magnetic saturation. A primary coil around another leg of the transformer has relatively low inductance as long as the magnetic saturation is maintained. But when a fault occurs, the system is designed so that the core is driven out of saturation by one polarity of the current. A second coil, connected in series with the first, is wound on a second yoke in the opposite sense and drives the yoke out of saturation with the other polarity of current. When the magnetic material enters its high permeability region near zero net applied field, its inductance becomes large, limiting the current.

This principle has been used to design and build several distribution-level saturated-core FCLs. One 35 kV prototype has been built by Innopower of Beijing China and installed in-grid at the Puji substation in Yunnan, alongside the 30 m cable described in Section 4. In-grid testing is beginning. Several others have been built by Zenergy Power, with a first 12 kV prototype installed in the Southern California Edison grid in March 2009.

These fault current limiters have the advantage of avoiding driving the superconductor normal and keeping the superconductor coil at ground potential; this dramatically simplifies the cryogenics compared to resistive FCLs. However, with two yokes per phase, the system is quite large, the primary coils add unwanted inductive impedance in normal operation and it scales with peak short circuit current, in contrast to bifilar wound resistive FCLs.

5.2 Resistive Type SCFCLs based on 1 G and 2 G Conductors

In 2005 Siemens Corporate Technology and American Superconductor Corporation formed a strategic alliance to develop and explore the commercialization aspects of HTS fault current limiters by building and testing FCL components based on AMSC's 4.4 mm wide second generation (2G) HTS wire [5.10]. In Jan. 2007 Siemens completed and tested a FCL module using AMSC's 344 superconductors, i.e. 2G HTS wire (YBCO coated conductor) with stainless steel stabilization [5.11].

The module corresponds to one phase of a 3-phase limiter for the 13 kV-class distribution voltage level. The basic specifications of the module are shown in Table 5.2. This resistive-type limiter implements a modular design consisting of 15 bifilar coils wound from a total of 15 times 50 m of 2G wire. According to Fig. 5.6 the modular design consists of 3 stacks connected in series, each stack containing 5 coils connected in parallel to adapt the limiter to the rated current and voltage. The size of the active part is about 40 cm × Ø 50 cm corresponding to a volume of 80 liters.

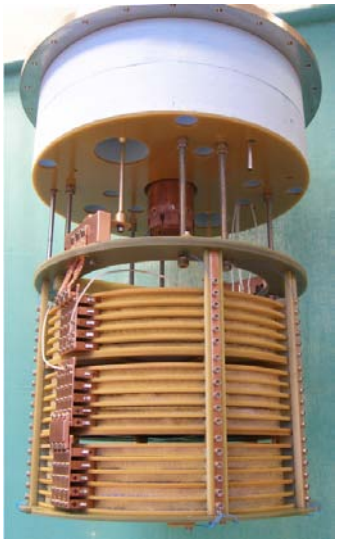

Fig. 5.6: Setup of the active part of the 2.25 MVA FCL module.

Table 5.2. Basic specifications of the single phase FCL module.

Rated current	300 Arms
Rated voltage	7.5 kVrms (13 kV phase-phase)
Nominal apparent power	2.25 MVA
Number of coils	15 = 5 x 3
Wire length per coil	50 m
Total length of wire	750 m
Wire width	4.4 mm
Type of wire	AMSC's 344S

The active part of the module was mounted into a liquid nitrogen bath-cooled cryostat operating at atmospheric pressure. The power tests of the fully assembled FCL module have been performed at the Institut "Prüffeld für elektrische Hochleistungstechnik" (IPH) in Berlin (Germany). In total more than 40 power tests at voltages between 6.5 and 7.8 kV have been performed in the standard configuration with the FCL directly connected in series between the source and a shortened load. The voltage was applied to the limiter for 40 to 50 ms depending on the phase angle at the start of the fault. Two series of power tests at different prospective short circuit currents of 10 kArms and 28 kArms respectively were performed with variation of the phase angle in steps of 15° between 0° and 150°. The peak let-through current under those conditions is shown in Fig. 5.7.

The peak current reaches its highest values between 60° and 90° and increases somewhat with the prospective current. For the 10 kA prospective current, corresponding to a typical grid with 3% relative internal impedance, the maximum

peak current is 6 times the critical current (I_c) of 430 A. The test with the highest peak current at 28 kA prospective current and 75° phase angle is shown in Fig 5.8. A maximum current of 7.3 times I_c is reached 0.5 ms after start of the fault. The resistance ratio shown in the lower diagram reaches a final value of 110%, corresponding to an average final temperature between 60 and 70°C. The peak limited current in the last half cycle of all power tests is about 2.4 times I_c.

In addition to the standard configuration, tests with an external reactor parallel to the FCL were performed. Using a reactor with impedance roughly equal to the source impedance of the test circuit, the test voltage could be increased to 8.3 kV, while the voltage across the FCL module dropped to about half of that value i.e. 4.3 kV. This proves that the active part of the FCL can be designed to be significantly smaller if operated in a shunted configuration.

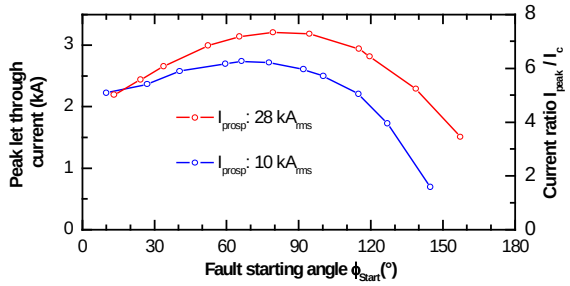

Fig. 5.7: Peak let-through current as a function of fault starting angle, absolute values (left axis) and values relative to I_c (right axis).

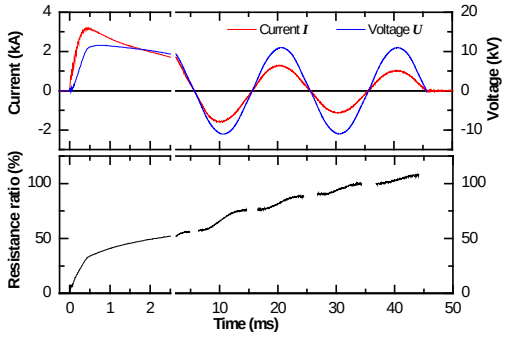

Fig. 5.8: Current, voltage and resistance ratio during a power test at 7.8 kV and a prospective current of 28 kA; fault starts at 75°.

Some of the tests were performed with a closed liquid nitrogen bath to monitor the pressure rise during a fault. Starting at atmospheric pressure the vent valves of the cryostat were closed 2 s before and re-opened 5 s after every fault. The pressure rise was measured and found to be below 400 mbar in all cases. This pressure range does not make special demands on the burst strength of the cryostat.

Finally, basic insulation level (BIL) tests of the standard rated lightning impulse and power-frequency withstand voltages have been performed. The insulation between the active part of the FCL and the grounded vessel was successfully tested at 95 kV (15 pulses 1.2 / 50 µs in both polarities) and at 38 kV (1 min, 50 Hz). These are the standard BIL levels for nominal voltages up to 17.5 kV.

In a follow-on project supported in part by USDOE, a 115 kV FCL is targeted by American Superconductor and Siemens, in collaboration with Nexans and Southern Cal Edison. A new, 1.2 cm wide stainless stabilized 2G wire has been developed and wound into bifilar coils. A distribution-level subscale module has been successfully tested in 2008, using tests similar to those described above. The advantage of the wider wire is that it reduces the number of coils which need to be wound and makes the system more compact, thus reducing cost. The project continues for a transmission-level single phase demonstration.

Another successful SCFCL laboratory demonstration was performed in Korea by Hyundai in collaboration with Yonsei University, also using AMSC 344 superconductors [5.22]. The single phase unit had an operating rating of 8.3 MVA and single phase voltage of 13.2 kV. Another significant Korean project was a 24 kV,

630 A three phase system developed by LS Industrial Systems in collaboration with Korea University and KEPRI [5.31]. This system was termed a hybrid fault current limiter because it featured the use of a series ultra-fast switch based on a vacuum interrupter with electromagnetic repulsion from current in a shunt circuit. The opening time was reduced to the msec range, which substantially reduced the energy dumped into the superconductor and the amount of superconductor required. Thin film HTS circuits were adequate in this case to provide the limiting. The main complication of this design is the use of a fuse which will limit the resetting time. The concept of a vacuum interrupter with electromagnetic repulsion as a series switch to limit energy dumped into the superconductor was first introduced and demonstrated by Tokyo Denki University [5.26].

In Japan, Toshiba reported construction and test a 6.6 kV demonstrator with 2G HTS wire [5.23]. In Italy, on the basis of a three-phase 3.2 kV, 1.2 MVA resistive-type SCFCL prototype successfully tested at CESI power laboratory at the end of year 2005 [5.12, 5.15], a new 9 kV, 1000 A SCFCL demonstrator, based on 1G HTS wire (Bi-2223 tape), has been designed. This SCFCL demonstrator is being to be manufactured and then installed, in 2010, in the MV public electric grid of the Milan area, for extensive field testing.

5.3 Resistive Type SCFCL based on MgB_2

In the years 2003-2005, several single-phase and a three-phase resistive-type superconducting FCL prototypes based on Ni-sheathed MgB_2 tapes, were designed, manufactured and tested in the framework of the Italian project LIMSAT [5.12]. SCFCL prototypes were made by 40 to 130-meters long MgB_2 tapes, wound on a cylindrical support made of fibreglass reinforced plastic (G10) obtaining anti-inductive windings that have been lapped with fibreglass tape and then impregnated with epoxy resin to avoid any possible radial displacement of the MgB_2 conductor occurring during short-circuit tests and/or repeated thermal cycling [5.13, 5.14].

Short-circuit tests were carried out at CESI test facility on MgB_2-based SCFCL prototypes cooled initially to 4.2 K and then, for the first time ever reported, at 27 K in a liquid neon bath by a closed-circuit refrigeration system that allowed a 3-day SCFCL testing without any neon depletion. [5.15].

Short-circuit tests have been performed for fault events of different severity, with prospective peak current I_{SC} up to 15 kA_p, and duration in order to estimate both the limiting capacity and the mechanical and thermal limits of the SCFCL prototypes at cryogenic temperatures. Results of short-circuit tests carried out on a 500 kVA-class SCFCL prototype show its fast current limiting action and the excellent current limiting capability of MgB_2 windings even after repeated fault events. Moreover, at nominal condition negligible voltage drop across the SCFCL has been detected, making the SCFCL device ‘transparent’ to the electric cuircuit.

The good technical performances (high critical current and resistivity matrix, thermal stability…) and the foreseen low-cost of MgB_2 tape make such conductor a good candidate for SCFCL applications, especially if refrigeration systems with enhanced efficiency and competitive price will soon become available. Otherwise, the relatively low operating temperature of MgB_2 increases the cryogenic load during normal operation, a critical factor for economic operation.

In the framework of a UK project called SuFCLEMP (Superconducting Fault Current Limiter for Electrical Marine Propulsion), which finished on March 2007, a single-phase 220V/1kA SCFCL prototype, using an innovative solid-state cooling system operating at 24-30K, has been developed [5.16]. It validated current sharing between parallel superconducting wires during FCL operation, and showed that high resistance monocore magnesium diboride wire was superior to heavily-stabilised multi-filament magnet wire for FCL operation at the first peak. The simplicity and stability of the system showed that the base technology matches a number of different FCL designs with different operational characteristics for different applications.

A new SCFCL and intelligent grid management project lead by Rolls-Royce Electrical Systems and Strategic Research Centre started in April 2007 with the final FCL device expected to be installed and test inside the Scottish Power grid. The project involves Diboride Conductors, the University of Manchester, Strathclyde University, Hyper Tech Research (Ohio) and Scientific Cryomagnetics (Oxford). The device will be a 3-phase FCL operating at distribution grid level.

5.4 Superconducting Fault Current Limiting Transformers (SFCLT)

A transformer with active current limitation can be realized with superconductors only and seems to be an attractive new device in the medium- to long-term range. Superconducting fault current limiting transformers (SFCLTs) have major benefits in comparison to conventional transformers.

(1) SFCLTs work as a transformer in normal operation, and also as an active fault current limiter in the fault condition.

(2) The leakage impedance of a SFCLT in normal operation is reduced, compared with conventional transformers. This improves power system stability, loadflow and voltage drops in the grid. Fault current limiting functionality is essential in this case; otherwise the low impedance would increase the fault current.

(3) SFCLTs are smaller and more lightweight than conventional transformers.

(4) SFCLTs are environment-friendly because of LN_2 instead of oil.

Test results of a 100 kVA HTS SFCLT

The specifications of a worldwide first HTS-SFCLT with 2G HTS material and its construction are shown in Table 5.3 and Fig. 5.9. A 3-phase demonstrator with

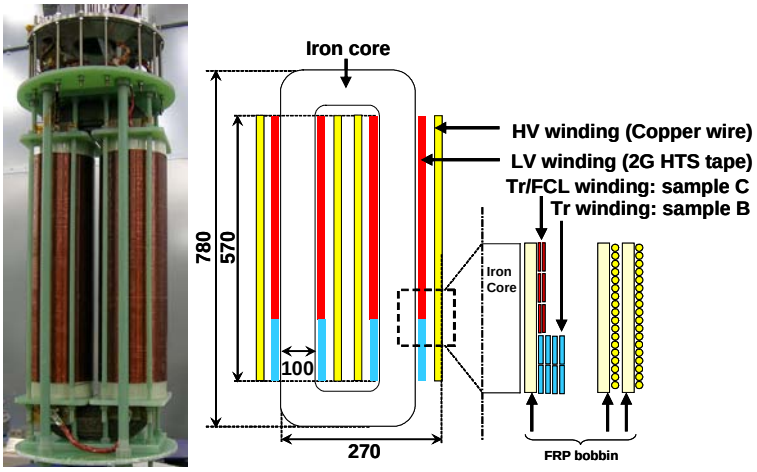

Fig. 5.9: 100 kVA HTS-SFCLT with 2G tapes

Table 5.3: Data of HTS SFCLT

Phase	3
Frequency	60 Hz
Capacity	100 kVA
Rated voltage	6.6kV/210 V
Rated current	8.7A/275A
Turn ratio	1344/74
Magnetic field	1.7 T
Leakage impedance	4.6%
Material LV(I)	YBCO
Material LV(II)	YBCO/Cu stab.

100 kVA and 6600V/210V was designed at Nagoya University, and a single phase device with 33.3 kVA and 3810V/210V was built and tested [5.17]. The low voltage coil consists of 2G HTS tapes, and the high voltage coil is composed of a 1.4 mm diameter copper wire. For simplicity the whole demonstrator was immersed in liquid nitrogen at 77K.

The transformer coil of the low voltage HTS coil is divided into 2 parts; limiting coil with current limitation function (Tr/FCL winding in Fig. 5.9) and non-limiting coil without current limitation function (Tr winding in Fig. 5.9). Such a hybrid construction of HTS coils has the benefit that the limiting impedance of the SFCLT is independent of the transformer design. With the variation of the ratio between the limiting Tr/FCL coil and the non-limiting Tr coil, HTS-SFCLT with 2G HTS material can perform the desirable current limiting characteristics as well as transformer functions.

The fundamental characteristics of SFCLTs have been verified through no-load and short-circuit tests in [5.18-5.21]. In this report the self-recovery characteristics of a SFCLT with 2G HTS wire is presented. This is an important feature of SFCLTs.

Figure 5.10 presents an example of low-voltage-side current (I_{LV}) waveform of SFCLT in the recovery test, where prospective current (I_{PRO}) is 980A_{peak}, load current before fault (I_{LV1}) is 112A_{peak}, and fault duration is 5 cycles. The fault current was limited to 516A_{peak} (52.6% of I_{PRO}) at the first peak and 330Apeak (33.7% of I_{PRO}) at the 10th peak, respectively, after the fault. In this case, the load current after the fault clearance (I_{LV2}) was equal to I_{LV1}, which means that the HTS coil at the low-voltage

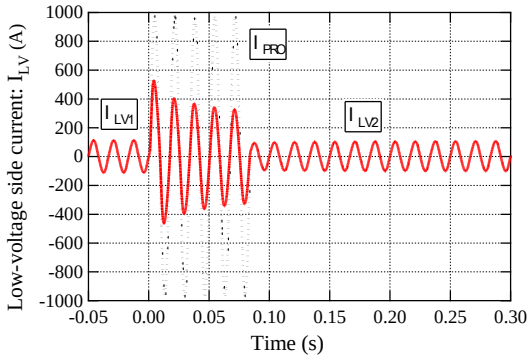

Fig. 5.10: Current waveform of recovery test for HTc-SFCLT with 2G coated conductors (I_{PRO} = 980 A_{peak}, I_{LV} = 112 A_{peak})

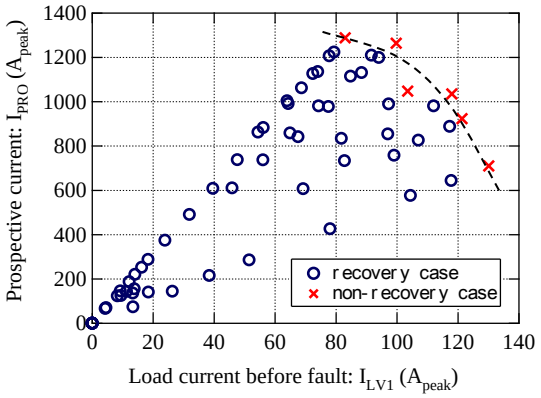

Fig. 5.11: Recovery characteristics of HTS-SFCLT with 2G coated conductors

side recovered into superconducting state by itself immediately after the fault clearance.

Figure 5.11 shows the recovery characteristics of the SFCLT as a function of I_{PRO} and I_{LV1}. The recovery into the superconducting state was defined as I_{LV2}/I_{LV1} > 99% in this experiment. The symbols ○ and X in Fig. 5.11 denote the recovery case and non-recovery case respectively. A broken curve can be found between the recovery and non-recovery cases, which can be regarded as the criterion or the limit of recovery for the HTS-SFCLT. In other words, when the load current (I_{LV1}) and the prospective fault current (I_{PRO}) were lower than those on the critical curve in Fig. 5.11, the HTS-SFCLT would recover into the superconducting state by itself immediately after the fault clearance.

As of spring 2009, a next generation SFCLT rated at 2 MVA/22 kV is prepared for test at Nagoya University.

5.5 State-of-the-Art of SCFCL Development

At present, many projects worldwide are on their way to develop prototype SCFCLs for further field tests, and the first commercial products are becoming available. An overview of the most recent and actual major SCFCL projects is given in Table 5.4. It can be seen that most of the projects follow the resistive type SCFCL and that recently more and more projects use 2G HTS wire (YBCO coated conductor) as the superconductor. The latter is mainly due to the progress in R&D of YBCO coated conductors and the availability of this material in adequate lengths since 2005.

Table 5.4. Important SCFCL projects (Status June 2009)

Lead Company	**Country/Year** [1)]	**Type**	**Data** [2)]	**Phase**	**Superconductor**
General Atomics	US / ´02	Diode bridge	12 kV, 1.2 kA	1-ph.	BSCCO 2223 tape
ACCEL/NexansSC	D / ´04	Resistive	12 kV, 600 A	3-ph.	BSCCO 2212 bulk
Yonsei University	Korea / ´04	Diode bridge	6.6 kV, 200 A	3-ph.	BSCCO 2223 tape
KEPRI	Korea / ´04	Resistive	6.6 kV, 200 A	3-ph.	YBCO thin films
CRIEPI	Japan / ´04	Resistive	1 kV, 40 A	1-ph.	YBCO thin films
Mitsubishi	Japan / ´04	Resistive	200 V, 1 kA	1-ph.	YBCO thin films
CAS	China / ´05	Diode bridge	10.5 kV, 1.5 kA	3-ph.	BSCCO 2223 tape
CESI RICERCA	Italy / ´05	Resistive	3.1 kV, 220 A	3-ph.	BSCCO 2223 tape
CESI RICERCA	Italy / ´05	Resistive	0.6 kV, 270 A	1-ph.	MgB2
Siemens / AMSC	D / US / ´07	Resistive	7.5 V, 267 A	1-ph.	YBCO coat. cond.
LSIS	Korea /'07	Hybrid	24 kV, 630A	3-ph.	YBCO coat. cond.
Hyundai / AMSC	Korea / ´07	Resistive	13.2 kV, 630 A	1-ph.	YBCO coat. cond.
KEPRI	Korea / ´07	Res.-hybrid	22.9 kV, 630 A	3-ph.	BSCCO 2212 bulk
Innopower	C / 2008	DC biased iron	35 kV, 90 MVA	3-ph.	BSCCO 2223 tape
Toshiba	J / 2008	Resistive	6.6 kV, 72 A	3-ph.	YBCO coat. cond.
Nexans SC	D / 2009	Resistive	12 kV, 100 A	3-ph.	BSCCO 2212 bulk
Zenergy Power	2009	DC biased iron	12 kV, 1.2 kA	3-ph.	BSCCO 2223 tape
Zenergy Power	2009	DC biased iron	15 kV, 1.2 kA	3-ph.	BSCCO 2223 tape
Nexans SC	D / 2009	Resistive	12 kV, 800 A	3-ph.	BSCCO 2212 bulk
Innopower	C / 2010	DC biased iron	220kV,300MVA	3-ph.	BSCCO 2223 tape
CESI RICERCA	I / 2010	Resistive	9 kV, 250 A	3-ph.	BSCCO 2223 tape
CESI RICERCA	I / 2010	Resistive	9 kV, 1 kA	3-ph.	YBCO coat. cond.
KEPRI	Korea / 2010	Resistive	22.9 kV, 3 kA	3-ph.	YBCO coat. cond.
AMSC / Siemens	2012 /US / D	Resistive	115 kV, 1.2 kA	3-ph.	YBCO coat. cond.
Rolls Royce	UK / -	Resistive	11.5 kV, 400 A	3-ph.	MgB_2

1) year of test
2) 3 phase systems phase to phase voltage / 1 phase system phase to ground voltage

Distribution voltage level SCFCLs

At the medium voltage level or distribution voltage level, the technical feasibility of the major SCFCL types has been demonstrated by several successful field tests (see section 5.1.1-5.1.3). The first commercial SCFCL applications for this voltage level are likely soon. Because of alternative technical solutions at the distribution level, the greatest challenge for distribution-level SCFCLs is cost reduction. In addition,

important issues for the future are to increase the performance of SCFCLs and to demonstrate long term reliability.

Recently, the progress in R&D on 2G HTS wire made it possible to realize compact resistive SCFCLs with low inductive windings. In Korea a successful high power laboratory short-circuit test with a single phase 13.2 kV, 630 A SCFCL demonstrator was performed in 2007 [5.22]. In March 2007 another successful test with a single phase 7.5 kV, 267 A SCFCL demonstrator was reported in Germany [5.11]. In Korea a so-called hybrid 13.2 kV, 630 kA SCFCL has been successfully tested in Nov. 2006. This type tries to minimize the amount of HTS material for SCFCLs. In Japan, Toshiba managed to construct and test a 6.6 kV demonstrator [5.23]. Another approach in Japan combines a vacuum breaker with a superconductor and this results in considerable superconductor savings [5.24]-[5.26] Depending on the future cost reduction of this wire and other system components, resistive SCFCLs with 2G HTS wire seem to be a compact and technically effective solution for medium voltage level SCFCLs.

Nexans SuperConductors has recently announced two commercial sales of distribution level SCFCLs based on their melt-cast Bi-2212 rods, one to Applied Superconductivity Ltd. in U. K., and one to Vattenfall for a substation in Boxberg, Germany. These are both 12 kV units, the first with 100 A rating, the second with 800 A rating. The first has been delivered and installed and is beginning operation as of spring 2009. The second is expected to be delivered during the summer 2009.

Many other resistive FCLs are under development, for example 9 kV, 250 A and 1000 A systems developed by CESI Ricerca in Italy, initially using 1G wire, and a relatively small system by AIST, Tsukuba, Japan, using thin film YBCO conductor on rigid substrates.

As stated earlier, all systems have advantages and disadvantages, and the practical systems will become clearer as testing continues.

Finally, it should be mentioned that fault current limiting functionality has also been introduced into other devices, such as cables, as described in Section 3, and transformers, discussed in section 5.4.

Transmission voltage level SCFCLs

A major reason to develop SCFCLs for the transmission voltage level is that there exists no conventional device with an active current limitation and low impedance during normal conditions. In addition, studies showed that high savings and many benefits can be achieved at this voltage level.

The first project to develop a HTS transmission type SCFCL started in 2003 in the US [5.27], involving SuperPower, Nexans and American Electric Power, and sponsored by USDOE. During the project it turned out that the concept of a so-called matrix type fault current limiter (MFCL), using rods of BSCCO-2212, is difficult to adapt to high voltage levels. As a result this project was discontinued for some time. In 2006, new partners, including Sumitomo Electric, joined this project and the concept was changed to a resistive SCFCL with 2G HTS wire (YBCO coated conductor). A successful intermediate test was reported in [5.28]; however this project has since been cancelled by SuperPower (Royal Philips Electronics) for reasons not publicly explained.

In 2005 a project called CULT-110 started in Germany with Nexans, FZK and E.ON to develop a 110 kV, 1.8 kA single phase resistive SCFCL by 2010. This project uses

MCP-BSCCO 2212 tubes with a magnetic field assisted quench concept [5.29]. The status and the concept are reported in [5.30]. A major challenge in this project is to develop the HTS component for all relevant short-circuit levels. However this project has also been cancelled.

In June 2007 the USDOE announced three new transmission level SCFCL projects [5.31]. One is the SuperPower/Sumitomo Electric project described above, now canceled. In the second project, a 138 kV three phase DC-biased (saturated) iron-core type SCFCL will be developed by Zenergy Power (SC Power). The third project, addressing a 115 kV three phase resistive-type SCFCL, extending the technology of the earlier Siemens/AMSC distribution-level demonstrator, links American Superconductor, Siemens, Nexans, Los Alamos National Laboratory and Southern California Edison.

Within the last phase of the Korean DAPAS program it is foreseen to develop a 154 kV SCFCL by 2010. It is not yet decided which type of SCFCL will be chosen. Intermediate successful tests with 22.9 kV demonstrators were performed with a hybrid type and a resistive type SCFCL, as described earlier. In China a first 220 kV fault current limiter based on the DC biased iron core concept is now planned for grid operation in 2010.

A major challenge for transmission level SCFCLs will be to demonstrate a reliable high voltage insulation concept for AC voltages and lightning impulses.

6 Superconducting Magnetic Energy Storage (SMES)

The energy in a SMES is stored in the magnetic field generated by a flow of a direct current in a superconducting coil. The absence of resistance of the superconductors makes this DC current persistent in short-circuited mode, although practical HTS superconducting contacts for a truly persistent switch have not yet been developed. By charging the magnet the energy is stored; it is recovered by the discharging of the magnet. An interface between the magnet and the load carries out the energy transfers. Since most loads operate in AC mode, this interface is in general a DC/AC converter (see Fig. 6.1).

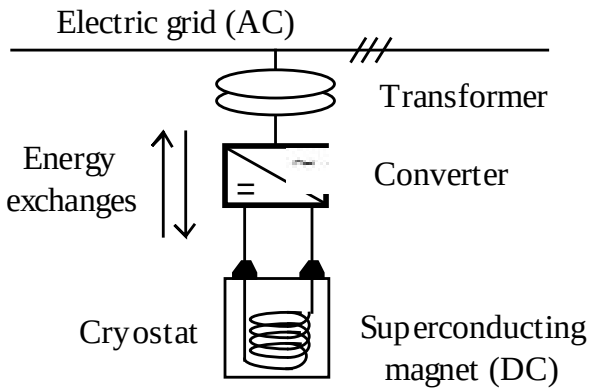

Fig. 6.1: Schematic drawing of a SMES linked to an AC grid.

The SMES system consists in four subsystems:

- SC magnet with its mechanical supporting structure.
- Cryogenic system (cryostat, vacuum pump, cryocooler, …).
- Power conditioning system (interface between the SC magnet and the load).
- Control system (electronics, cryogenics, magnet protection, …).

How does SMES compare with the other energy storage systems? The stored energy is mainly limited by mechanical considerations. The Virial theorem [6.1] gives the upper limit for the magnetic energy per unit structural material volume: it is simply the operating stress. With a “reasonable” stress of 100 MPa the magnet cannot store more than 100 MJ/m^3 (30 kWh/m^3) or 12 kJ/kg (3.5 Wh/kg) for steel. The operating stress may be increased but the energy capacity of a SMES is anyway limited. Batteries offer better storage energy density but SMES shows better power capacity. Another key factor is cost. Ultracapacitors are increasingly commercially available and may create significant cost competition for SMES in the future; unless the magnetic field level is significantly increased above the 10 T level, ultracapacitors also offer higher energy density when one takes into account the cryogenic and mechanical infrastructure of SMES, but require many units in series to achieve adequate voltage. Flywheels form another competitive technology.

A superconductor magnet can release its energy very quickly and its power density can be very high. For the magnet, the operating current (I_o) and the maximum voltage (V_{max}) allowable across it limit the power (I_o V_{max}). The SMES performances in terms of power densities are extremely high, much higher than batteries.

The magnet charge can be significantly slower than the discharge. The number of possible charge-discharge cycles is very high since it is mainly limited by mechanical fatigue. A SMES may then be used for repetitive and rapid power bidirectional exchanges with the load. The energy loss for a discharge (or charge) can be kept to some % of the stored energy through a suitable HTS wire design in order to minimize the AC losses. The SMES energy conversion is then excellent with possible values higher than 95 %.

The SMES characteristics (high power, reasonable energy) make its use particularly interesting for storage systems of high powers (MW and higher) and short discharging times (ms to s). An overview of SMES is given in [6.2]. However, applications in the power grid must be studied carefully to determine whether real power is required to meet a utility need. In many case, dips and sags in voltage involve inductance and can be compensated by capacitive reactive power. In those cases, power electronic devices like Static VAR Compensators or statcoms can also do the job.

6.1 Field Test Experience with LTS SMES

6.1.1 25 MW SMES based Pulsed Power Modulator

In view of disturbances of the electrical power grid, it is often required to buffer pulsed power loads by the use of energy storage. A practical example is the supply of the large number of klystrons of linear accelerators like TESLA or ILC.

Based on a SMES, a long-pulse klystron modulator has been developed for use in the TTF at DESY [6.3]. The patented system is capable of serving either one multi-beam klystron of 10 MW output or two standard klystrons of 5 MW output each with a maximum average power of 440 kW. The data on the SMES coil are given in Table 6.1 and the superconducting coils of the SMES are shown in Fig. 6.2.

One important aspect of the design was the safe operation of the valuable klystrons under all conditions. In case of klystron arcing, the big inductance of the SMES (here 70 mH) is an inherent effective limiter of increasing short-circuit currents, assisted by protection circuits. A crowbar system with an ignitron is not required. Rapid control of the protection system is not needed either.

For further improvement of safety, a special protection device has been developed for insertion into the secondary circuit.

Fig. 6.2: SMES coils for 25 MW pulsed power modulator

Table 6.1 Pulse and coil data

Pulse data	
Pulse length	1.7 ms
Pulse power	17-25 MW
Frequency	5-10 Hz
Flat top	± 0.5 %
Coil data	
Inductance	70 mH
Magnetic field	4 T/2600 A
Max. voltage	7 kV
Max. dB/dt	100 T/s
Stored energy	237 kJ

6.1.2 5 MVA SMES for Bridging Instantaneous Voltage Dips

A large factory manufacturing liquid crystals or semiconductors requires a highly reliable power system, as well as a system that compensates for instantaneous voltage dips all around the factory. The SMES system, which is capable of supplying high power output and controlling storage capacity in an unrestricted manner, is possible solution. The SMES system is capable of immediately supplying high power output, which is the most desirable feature to compensate for instantaneous voltage dips.

An instantaneous voltage dip-bridging SMES system with an output of 5 MW was fabricated in 2003 by Chubu Electric Power Co. and collaborators in Japan. The SMES system consisted of an LTS coil, quench detector, protective resistor, high-speed switch, converter, and cryocooler, with the rated output of 5MVA and the output duration of 1 second, for protection from instantaneous voltage dips [6.4]. Data concerning the superconducting coils is shown in Table 6.2, and the appearance of superconducting coils is outlined in Fig. 6.3.

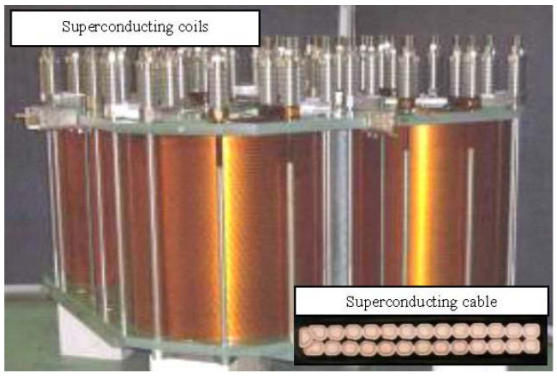

Fig. 6.3: Superconducting coils (5-MVA SMES)

Table 6.2: Main specifications of the coils (5-MVA SMES)

Coil arrangement		4-pole config.
Coil figure		Solenoid
Rated current		2,657 A
Rated voltage		2.5 kV
Inductance		2.08 H
Stored energy		7.34 MJ
Utilized energy		5 MJ
Maximum field		5.3 T
Coil size	Inner radius	0.265 m
	Outer radius	0.324 m
	Height	0.700 m

In July 2003, a verification test of an instantaneous voltage dip-bridging SMES system with 5MVA output was started in an advanced factory manufacturing liquid crystals in Japan [6.5]. This system was verified to compensate for several instantaneous voltage dips during the period between July 2003, when the verification was started, and May 2006, when it was completed. An example of the bridging voltage waveform for instantaneous voltage dips caused in the power

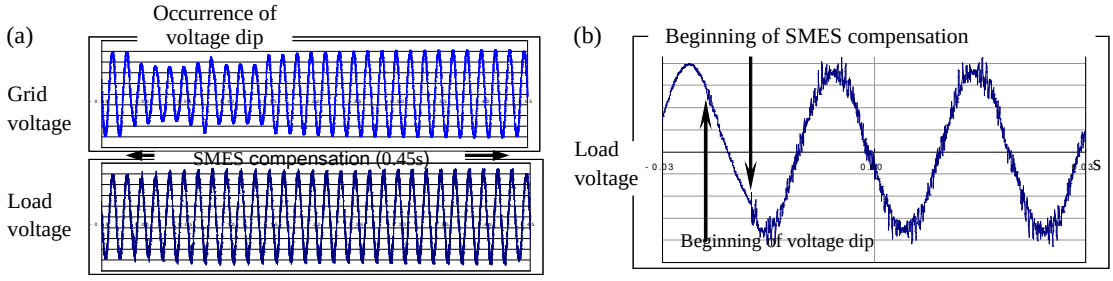

Fig. 6.4: Voltage transitions in an actual compensating operation (5 MVA SMES); (a) overall figure, (b) enlarged figure.

system, including the testing site by the lightning that frequently occurred in September 2004, is given in Fig. 6.4. The normal voltage level was immediately recovered by the power supply from the SMES system to support important systems at the factory without affecting any load in the factory.

6.1.3 10 MVA SMES for Bridging Instantaneous Voltage Dips

Another SMES system with the rated output of 10MVA and the output duration of 1 second was fabricated, and its field test started in the same testing site in October 2005. Data concerning the superconducting coils as energy storage units of the system is shown in Table 6.3, and the appearance of the coils is outlined in Fig. 6.5.

The SMES system can increase output capacity by raising the withstand voltage of the coils. The higher withstand voltage, in turn, permits a reduction of the coil current to decrease power loss from the coils and reduce the current lead size, thus resulting in a reduced heat transfer from the outside and improved standby efficiency. In addition, the system is constructed to compensate for instantaneous voltage dips caused by successive occurrences of lightning.

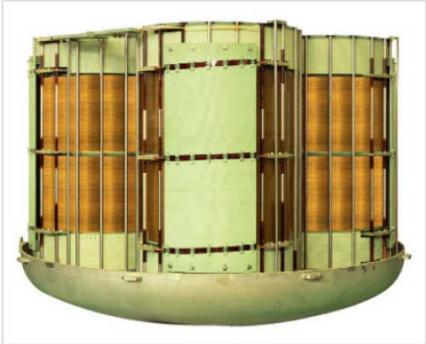

Fig. 6.5: LTS-Superconducting coils (10 MVA SMES)

Table 6.3: Main specifications of the coils (10 MVA SMES)

Coil arrangement		4 pole configuration
Coil figure		Solenoid
Rated current		1,400 A
Rated voltage		DC 6.6 kV
Inductance		21.1 H
Stored energy		20.7 MJ
Utilized energy		10 MJ
Maximum field		4.13 T/4.44 T
Coil size (A type/ B type)	Inner radius	0.346 m/0.410 m
	Outer radius	0.404 m/0.468 m
	Height	0.194 m/0.495 m

With an instantaneous voltage dip-bridging SMES system with the output of 10MVA, several sound compensating actions have also been verified so far. The voltage amplitude transitions at the grid and at the load during the compensating operation in July 2006 are illustrated in Fig. 6.6.

6.1.4 2.6 MJ, 2 MW SMES for Power Compensation

American Superconductor (AMSC) has the broadest experience worldwide with SMES in a utility environment, with nine SMES systems which were installed in 2 grids in the United States: 7 in Wisconsin on the 115 kV Northern loop now run by American Transmission Company and 2 in the Entergy 138 kV grid in Texas. In fact, until recently, this product was the only truly commercial (not government-supported) superconductor product for the power grid.

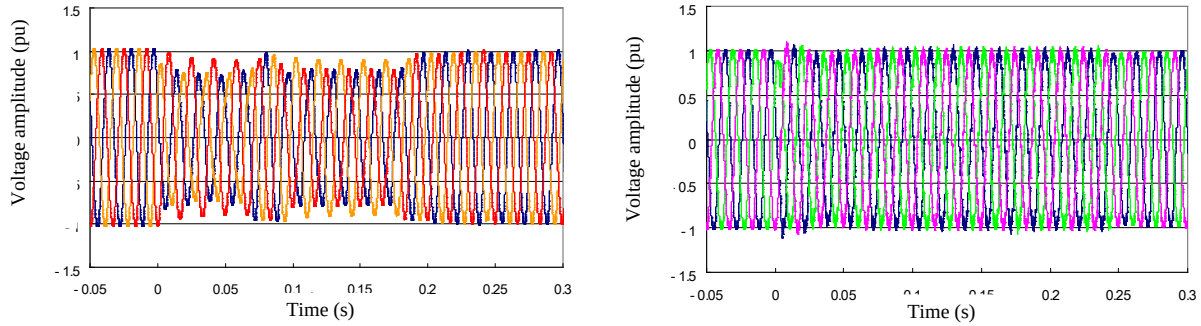

Fig. 6.6: The load side (left figure) and the grid side (right figure) voltage amplitude transitions in an actual compensation operation (10 MVA SMES).

These units have 2.6 MJ magnets fabricated with NbTi LTS superconductor, capable of discharge in the range of one second, thus providing real power of over 2 MW. The magnets are coupled to a power electronic system with a dc bus operating at 3000 volts and IGBT based power conversion providing a combination of real (in-phase) and reactive (out-of-phase) AC power. The systems are packaged in trailers, providing convenient mobility to adapt to changing utility conditions, and are located within substations on the medium voltage low side of distribution transformers. The cryogenic system consists of liquid helium in a closed refrigeration loop with two-stage 4.2 K cryocoolers, which require only limited maintenance. The systems have been in successful operation for over six years but have recently been decommissioned.

However AMSC has discontinued offering new SMES systems because of low utility interest in the SMES capability in the megawatt range and their preference for a purely power-electronics-based system providing reactive power compensation for grid stability, industrial power quality and wind farm power regulation. Therefore AMSC has moved its commercial focus to purely power-electronic-based systems, called D-VAR®; these have been broadly successful in the United States, Canada, United Kingdom, Australia and a number of other countries.

The reason for this lack of interest in SMES appears to be a combination of two factors: 1) the expense of the superconductor magnets over and above the expense of the power electronics, and 2) the predominantly reactive nature of the grid, at least in the United States, during power disturbances which can be largely compensated by reactive power without real power. While rapid injection of real power from the SMES energy storage can be critical in certain specific applications, it is not clear at this point whether the range of such applications is sufficiently broad to support commercial SMES in the megawatt range.

6.1.5 1 MVA SMES for Power System Control (Load Fluctuation Compensation)

In a national project in Japan, the technology for the HTS coils of the SMES system for load fluctuation compensation, frequency control and power system stabilization was established before 2003, and it was verified that cost reductions would be feasible.

In the ongoing project started in 2004, a model power electronic converter with the output of 20 MVA was manufactured to verify the core technology for 100MW-class power system, aiming to realize a low-cost, large-capacity converter as a major component (in addition to the superconductor coils). A SMES system containing this converter was connected with an actual power system to verify its load fluctuation compensating and system stabilizing functions. The evaluation items include:

a. Repeated operation for 20,000 or more cycles

b. Control responsiveness and operating properties

c. Failure detection and monitoring functions

d. Impacts on the network during SMES operation

The power system connection test was scheduled to continue for six months (including the conditioning period) during the fiscal year of 2007, and it was conducted by connecting the SMES with a hydroelectric power plant in a domestic

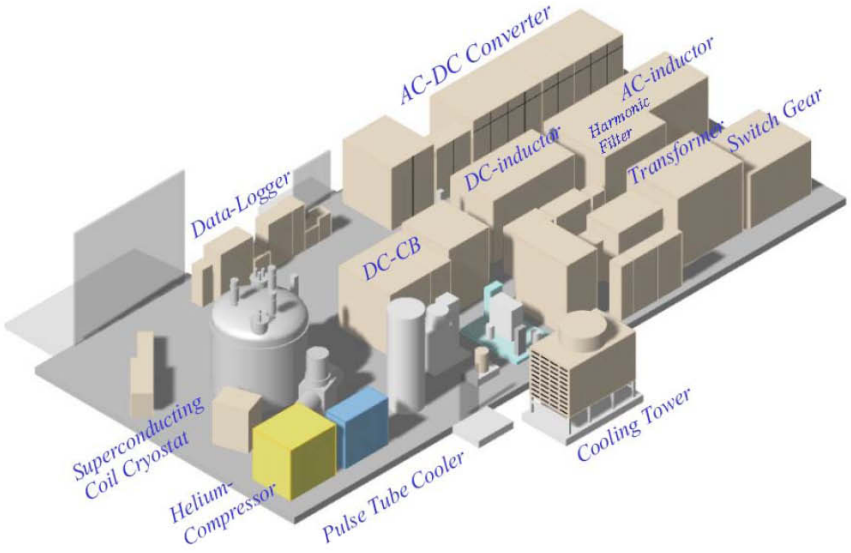

Fig. 6.7: Overhead view of the SMES system layout.

metal rolling factory. An overhead view of the SMES system layout is shown in Fig. 6.7.

6.2 State-of-the-Art of HTS SMES Development

6.2.1 800 kJ HTS SMES for Pulsed Power Applications

SMES is a very interesting energy storage device for pulsed power sources due to its high power density. An electromagnetic launcher or rail gun requires such a very high pulsed power supply. Furthermore SMES as current source suits better to an electromagnetic launcher than the presently used capacitors, which are voltage sources.

The conversion factor has the potential to be much higher with SMES as compared to capacitors. However extensive research and developments are still required to make SMES available for electromagnetic launchers. HTS SMES appears more suitable than LTS SMES in severe military environments because of its greater

stability and simpler cooling requirements. Repetition rate of the application is a critical issue, since ac losses during discharge need to be dissipated. A SMES of a few hundreds of kJ at a temperature of 20 K with integrated cryogenics is an intermediate phase, which remains essential to develop the basic technologies for manufacturing HTS SMES [6.6]. The purpose is to qualify several technological solutions on a representative level and to acquire an essential operational experience. The two key elements are a HTS conductor adapted to SMES and a transparent cryogenics for the user, i.e. without cryogenic fluid handling.

Figure 6.8 shows the HTS SMES made in Grenoble by the CNRS with the support of the DGA (Délégation Générale pour l'Armement). The basic element of the conductor is a powder-in-tube tape with the bismuth 2212 stoichiometry ($Bi_2Sr_2CaCu_2O$ – Bi 2212) produced by Nexans [6.7]. A conductor was fabricated from 3 or 4 tapes soldered together. The number of tapes is adapted to the local magnetic flux density within the magnet. In locations with high electromagnetic stresses the conductor has

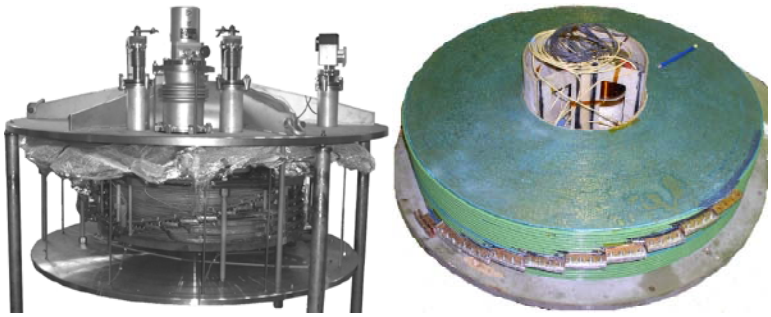

Fig. 6.8: 800 kJ HTc (Bi-2212) SMES with the 26 pancake magnet cooled by conduction.

Coil in its cryostat (left) and pancake coil under assembling (right)

a stainless steel tape to reinforce it: the allowable stress of the tape is otherwise too low (100 MPa).

The coil consists in 26 superposed simple pancakes wound and bonded on cut copper plates coated with epoxy. The rated current is 315 A for an energy of 814 kJ. The external diameter of the coil is 814 mm and its height 222 mm. The maximum magnetic flux densities are 5.2 T and 2.5 T respectively in axial and radial directions. The cooling at 20 K is performed by conduction from a cryocooler to make cryogenics very simple and transparent. A second cryocooler cools the current leads and the thermal shield. The thermal system operates in a satisfactory way and in agreement with the calculations. The tests of the magnet were conclusive even if the energy of the theoretical design was not still reached. For the current, 80% of the rated value was recorded (244 A). With resistive discharges from this current, a maximum power and energy of 175 kW and 425 kJ have been recorded. Fast discharges showed that the losses in the magnet and its close environment are low; the rises in temperature are very limited.

6.2.2 1 MVA HTS SMES for Bridging Instantanous Voltage Dips

The majority of the SMES systems described above use low temperature superconductor (metallic) coils. To reduce SMES costs and size in the future and to make it easy to maintain, it is necessary to develop an SMES system adopting a high-temperature superconductor that does not use liquid helium for cooling. Chubu Electric Power Co. and collaborators in Japan were engaged in the development of an SMES system using a Bi-2212 oxide superconductor. The Bi2212 oxide

superconductor maintains excellent energizing properties even in a strong magnetic field (Fig. 6.9) and has a higher critical temperature and, consequently a larger temperature margin, permitting the realization of a compact SMES system with a higher thermal stability with the use of a strong magnetic field, which would be difficult to realize using a metallic conductor.

Not being restricted by the refrigerant, electric insulators for the coils can be designed separately. Chubu Electric Power tested 1MVA-class instantaneous voltage-dip-bridging SMES coils with energizing capacity in the order of 2,500A at 4.2K in a self-generated magnetic field [6.8], [6.9].

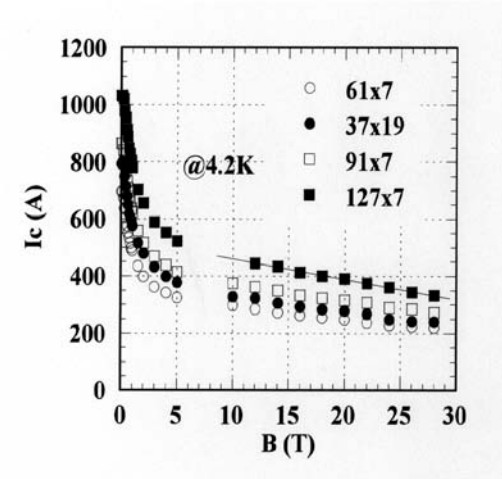

Fig. 6.9: Magnetic field dependency of critical current, I_c of Bi2212.

Those SMES coils used a conductor consisting of six twisted &1mm-diameter Bi-2212 wires manufactured by Showa and wound around a nickel-chromium alloy wire into a short solenoid, and a heat-conducting aluminum panel was put between each pair of coils so as to stack 18 coils. With this method, coils can be manufactured with a fixed conductor length and a heat-conducting panel located between each pair of coils, with the coil stacking order changeable according to the magnetic field properties of the conductor. The coil data are shown in Table 6.4, the appearance of 1 MJ class coils in Fig. 6.10, and a 1 MVA SMES system for bridging instantaneous voltage dips is outlined in Fig. 6.11.

Fig. 6.10: A 1MJ-class SMES coil for bridging instantaneous voltage dips.

Table 6.4: Main specifications of the coil (1 MVA SMES)

Coil figure	Stacked single solenoid coil
Coil size	0.38(ID)×0.70(OD)×0.554(H) m
Coil turns	6 turns× 49 layers ×18 stacked
Rated current	500 A
Rated voltage	2,500 V
Inductance	7.87 H
Stored energy	984 kJ

This system was evaluated by an instantaneous voltage-dip-bridging test using a simulated 1MW load resistor, and a multi-lightning test for the required response of the bridging system to the lightning. Those tests showed that the coil temperature could be controlled as designed, even if the power was shut off in the most severe manner to the continuous compensating actions and coils, and gave evidence of higher thermal stability thanks to the characteristics of the oxide superconductor [6.10].

However, challenges such as improving energizing properties and the strength of a longer conductor are still to be met before the SMES can be put to practical use, and those improvements must be accomplished so as to realize a low-cost, compact SMES system.

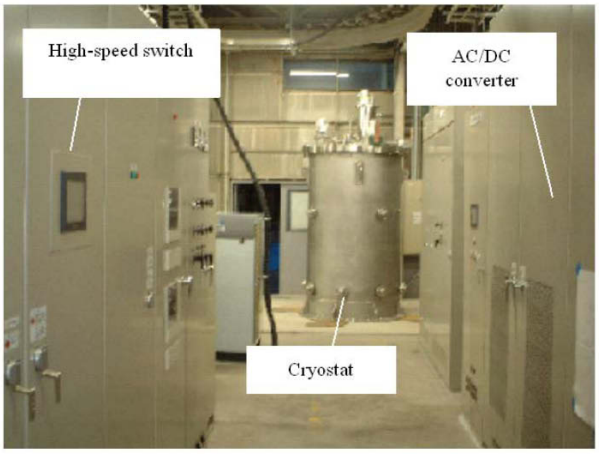

Fig. 6.11: A 1MVA SMES system for bridging instantaneous voltage dips.

6.2.3 R&D on 20 MJ class HTS SMES

2G HTS wires (YBCO coated conductor) have been developed and have shown remarkable progress in recent years through increasing wire length and amperage. SMES coils using 2G HTS wires have also been developed in a project started in 2004 in Japan [6.11]. The critical current density as a function of magnetic field for different types of superconductor material in wires is shown in Fig. 6.12. It can be seen that the YBCO material in 2G HTS wires, even at 50 K, has superior properties

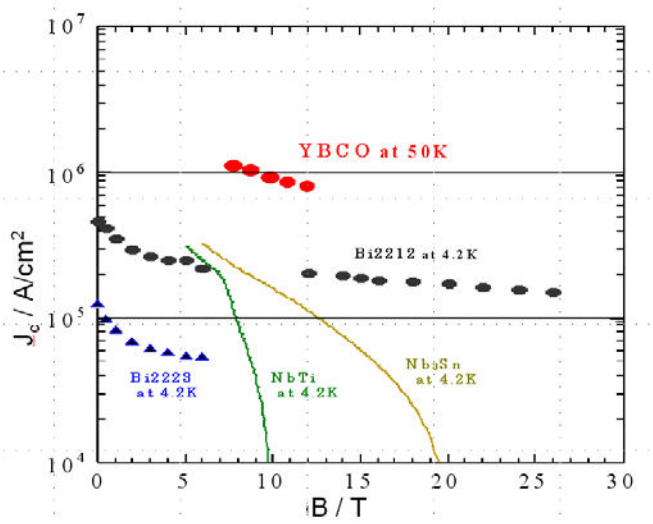

Fig. 6.12: Magnetic field dependency of critical current density, J_c.

to those of other superconductor materials at the liquid helium temperature of 4.2K, and thus in principle they open up an opportunity for a better energizing performance at higher temperatures and in a stronger magnetic field. However it must be recognized that the YBCO layer in a coated conductor is typically very thin, of order a micron, and so the engineering current density is one to two orders of magnitude lower. Thus significant development work is still required to realize the potential advantage. Another advantage of YBCO coated conductors using hastelloy substrate is their tensile strength in the order of 1G Pa needed for high energy density.

A 20 MJ HTS SMES for bridging instantaneous voltage dips is compared with a LTS SMES in Fig. 6.13. Further cost reduction and reliability improvement, which must be accomplished to put SMES into practical use, can be realized through a field strength increase and size reduction of the coils along with operation at higher temperatures.

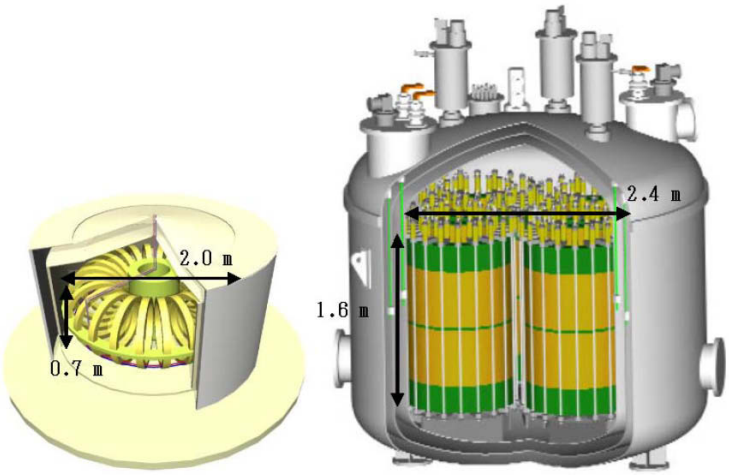

Fig. 6.13: Comparison of 20MJ-class SMES coils.
Left: YBCO SMES with 20 K cryocooler cooling
Right: NbTi SMES with 4 K helium pool boiling cooling system

7 Electrical Insulation

7.1 Introduction

Research and development of HTS power apparatus have been accelerated in the world and many field tests underlined the superior technical performance of HTS power devices. However, several failures due to dielectric breakdown have been reported in their performance tests [7.1-7.3]. The investigation of the failure of a DOE-sponsored HTS transformer project in the US by Waukesha Electric Systems and SuperPower concluded “a dielectric manufacturer should be a partner” and “HV expert must be on-site at coil manufacturer” [7.1].

In this context, electrical insulation technology of dielectrics at cryogenic temperature, i.e. cryodielectrics, has been recognized as one of key and common technologies for the practical development of HTS power apparatus. Dielectric characteristics of liquid nitrogen (LN_2) are fundamental for many HTS power applications. For the practical and reliable insulation design of HTS power apparatus, composite insulation systems composed of LN_2 and solid dielectrics such as paper and epoxy are important. In addition, gaseous nitrogen (GN_2) and vacuum at cryogenic temperature play an important role for conduction-cooled HTS power apparatus.

According to the recent project reports on HTS power applications, the applied rated voltages for HTS equipment are going to be enhanced, such as , 115 kV FCL and 138 kV cable in USA, 154 kV FCL in Korea, and 275 kV cable in Japan. The playing role of electrical insulation techniques in HTS equipment is becoming enhanced [7.25].

This paper reviews the state-of-the-art activities in research and development on cryodielectics together with the advanced techniques for discharge measurement. Especially, partial discharge (PD) characteristics as the precursor leading to breakdown (BD) are a focus in order to elucidate the physical mechanisms of discharge inception and propagation or insulation degradation.

7.2 Electrical Insulation of Power Apparatus

7.2.1 Insulation Component

For electrical insulation design of HTS power apparatus, insulation tests should be carried out as in the case of conventional technology. At the same time, one has to introduce and establish the concept of safety margin in order to obtain the operational feasibility and the longest lifetime under cryogenic environment. The conventional concept of insulation coordination should be kept, including overvoltage analysis on ac voltages and surges which occur also in the HTS system. Investigation of insulation coordination allows one to determine the relationship between the ratings of the HTS power apparatus and the test voltage.

Since transformers include many kinds of insulation types and in general tend to be exposed to high voltage conditions, let us take the transformer as example. Figure 7.1 shows the classification of the insulation design in a HTS transformer [7.4]. Although Fig. 7.1 basically resembles a conventional oil-filled transformer, it also contains some elements peculiar to cryodielectrics. In order to clarify insulation characteristics in each part ①–⑨ in Fig. 7.1, many insulation characteristics of cryogenic liquids should be experimentally investigated. As the common and

fundamental insulation characteristics for ①–⑨, this summary focuses mainly on the following:

- Area and volume effect
- Pressure dependence
- V-t characteristics
- Quench-induced insulation characteristics

at breakdown or PD inception in cryogenic liquids and/or composite insulation systems for HTS power apparatus.

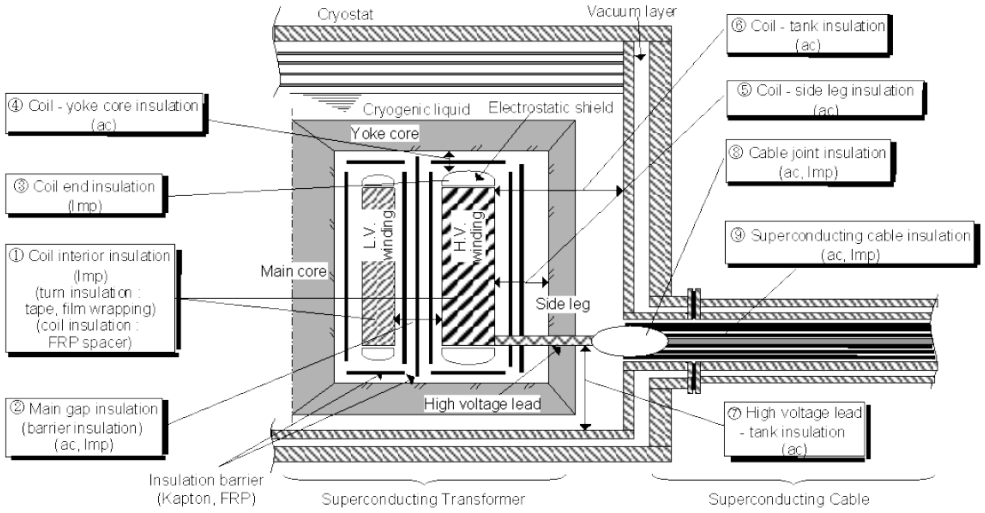

Figure 7.1: Classification of the insulation design in a HTS transformer [7.4]

7.2.2 Flowchart for Electrical Insulation Design

Figure 7.2 shows a flowchart for electrical insulation design of HTS power apparatus, taking into account the insulation characteristics described in later sections [7.4]. At first, the electric field calculation is carried out for the determination of the specifications of the power apparatus (electrode configuration, gap length and so on). Next, in part (a), the breakdown stress level is evaluated from the viewpoints of area and volume effects, together with the creepage discharge characteristics at the interface of cryogenic liquid/solid insulators. In part (b), V-t characteristics are considered with the testing voltage. For the reliable and practical insulation design of HTS power apparatus, it is necessary to examine the factors peculiar to cryogenic liquids as listed in part (c); e.g. quench-induced dynamic insulation characteristics. For the breakdown stress level evaluated from the considerations peculiar to cryogenic liquids, some sort of coordination with system conditions should be considered in part (d). Moreover, the breakdown margin should be determined from the breakdown scattering. Through the above discussion and procedure in Fig. 7.2, the reliable electrical insulation design of HTS power apparatus can be completed for practical use.

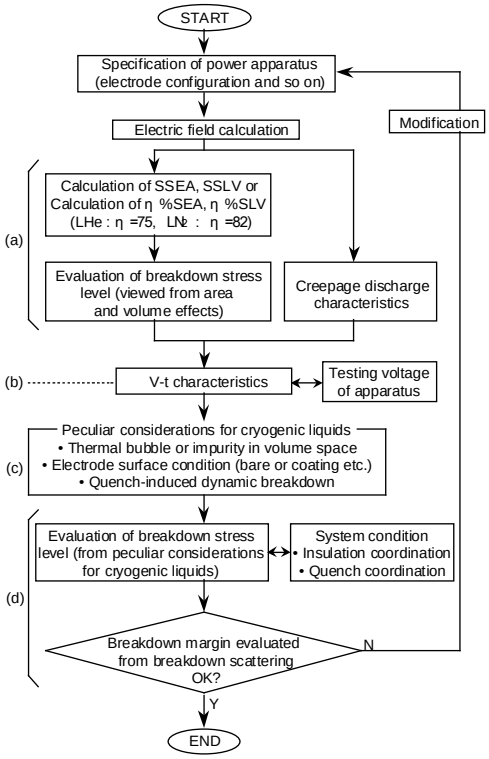

Fig. 7.2 A flowchart for electrical insulation design of HTS power apparatus [7.4]

7.3 Dielectric Characteristics of LN_2 and GN_2

7.3.1 Dielectric Materials at Cryogenic Temperatures

Fundamental electrical insulation characteristics of cryogenic liquids are reviewed by Gerhold [7.5]. Dielectric measurements were carried out with different classes of LN_2 purity. Figure 7.3 shows the breakdown probabilities as a function of the breakdown voltage [7.6]. The evaluation of the measurements showed that the breakdown voltage for humid LN_2 is 59 kV, for pure LN_2 62 kV and for the filtered LN_2 61 kV. Considering the slope of the approximation lines in Fig. 7.3, the slope of the humid line is low and starts with high values at low voltages. This means that very low but also very high breakdown values can be achieved depending on the flow conditions of the ice particles between the electrodes. This is the reason for a higher variance of distribution for humid LN_2 (9.5 %) comparing to the other two classes (6.5 %).

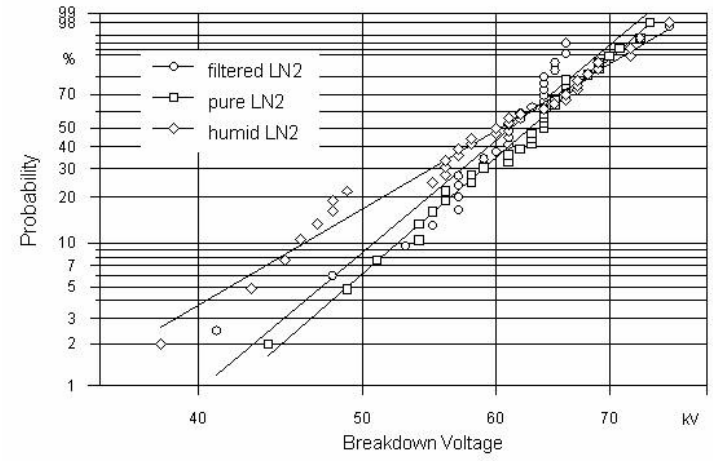

Fig. 7.3 Breakdown probability of different LN_2 classes [7.16]

7.3.2 Partial Discharge Measurement

Partial discharge (PD) or pre-breakdown phenomena in LN_2 must be understood for the reliable insulation design and diagnosis of HTS power apparatus. Recent electrical and optical techniques for PD measurement enabled detection of PD signals with high sensitivity and high resolution. Figure 7.4 shows the PD propagation characteristics of a long-gap, non-uniform (point-plane) geometry in LN_2 under impulse voltage application [7.7]. The streak photograph with the corresponding PD light intensity signals makes clear the filamentary PD propagation up to the plane electrode. The positive streamer in Fig. 7.4 (b) propagated faster and longer than the negative streamer in Fig. 7.4 (a).

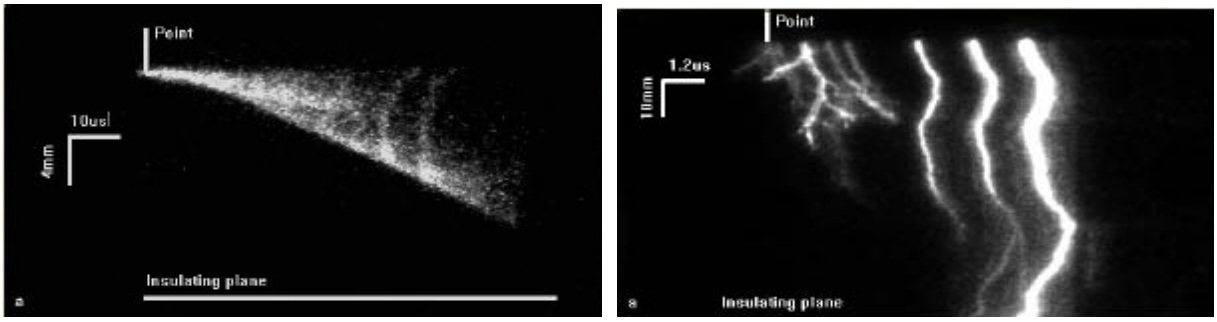

Fig. 7.4: PD propagation characteristics in LN_2 [7.7]
(long gap, non-uniform geometry)
Left-Negative impulse (Va=-101 kV, d=20 mm)
Right-Positive impulse (Va=+102 kV, d=80 mm)

PD measurement reflects their physics and their current pulse waveforms. The reason is that the rise and fall times of a PD current pulse waveform are directly determined by electron avalanche and/or streamer/leader discharge extension, and by diffusion and recombination of charge carriers, etc. From this viewpoint, a useful PD measurement and analysis technique referred to as “PD Current Pulse Waveform Analysis (PD-CPWA)” has been developed [7.8]. PD-CPWA can obtain not only individual PD current pulse waveforms with the time resolution of the order of sub-nanoseconds, but also its time transition from PD inception to breakdown, with the PD detection sensitivity of 0.1 pC. The obtained PD current pulse waveforms can also be analyzed in terms of different parameters such as peak value, di/dt, rise time, fall time of a single PD pulse, time interval of subsequent PD pulses and so on.

7.3.3 Fundamental Dielectric Characteristics of LN_2

Fundamental dielectrics characteristics of cryogenic liquids are introduced in this sub-section for the practical development and insulation design of HTS power apparatus. Dielectric characteristics of composite insulation systems composed of cryogenic liquids and solid dielectrics will be described in the next sections.

(a) Area and volume effect on breakdown strength

Discharges in conventional power apparatus can be caused by weak points such as micro-protrusions on the surface of electrodes in SF_6 gas, bubbles and impurities in insulating oil. Since the effect of such weak points depends on electrode size, discharge probability or dielectric strength of the power apparatus decreases with the increase in area and volume with high electric field strength. These phenomena are well known as the “area effect” and the “volume effect” on dielectric strength, generally taken into account in the practical insulation design of conventional power apparatus.

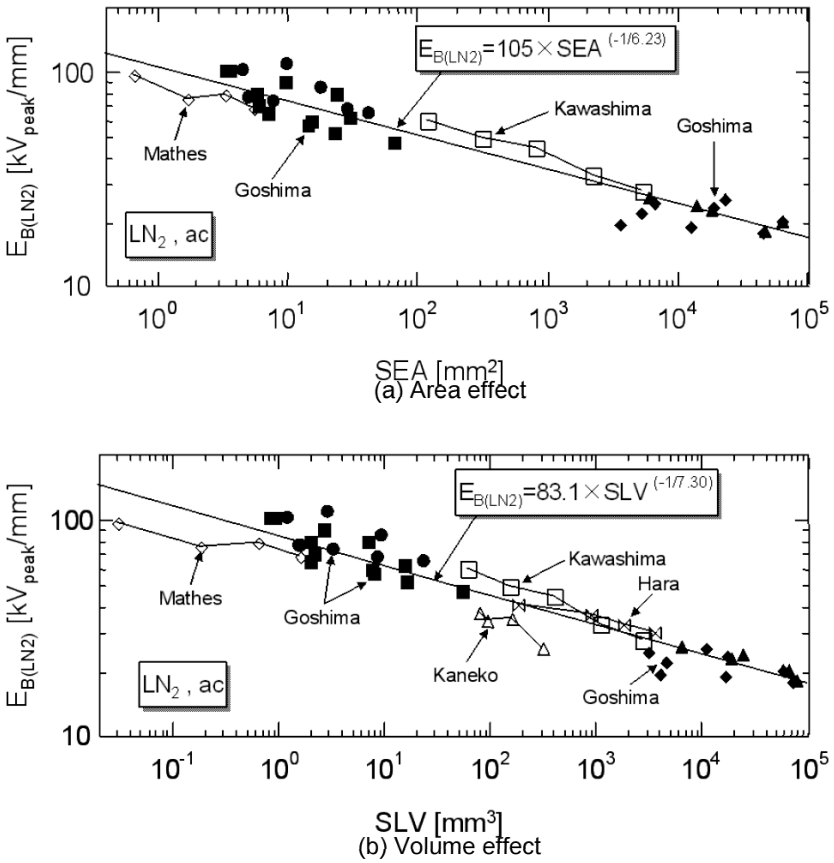

Fig. 7.5 Area and volume effect on breakdown strength in LN_2 [7.4]

Area and volume effects on the breakdown strength of LN_2 were systematized by compiling data from different bibliographic sources. Figure 7.5 shows ac breakdown strength EB (LN_2) of LN_2 at atmospheric pressure as a function of (a) SEA (stressed electrode area), i.e. area effect, and (b) SLV (stressed liquid volume), i.e. volume effect [7.4]. Breakdown strength in LN_2 decreased linearly in a log-log scale with the increase in SEA and SLV over extensive ranges (SEA: 10^{-1}-10^5 mm^2, SLV: 10^{-2}-10^5 mm^3).

Area and volume effects on the ac breakdown strength of LN_2 can be expressed by

Area effect: $E_{B(LN_2)} = 105 \times SEA^{-\frac{1}{6.23}} [\mathrm{kV_{peak}/mm}]$

Volume effect: . $E_{B(LN_2)} = 83.1 \times SLV^{-\frac{1}{7.30}} [\mathrm{kV_{peak}/mm}]$

Since SEA and SLV are geometrically related, further investigations were conducted to determine whether area effect or volume effect has greater influence on the breakdown characteristics of cryogenic liquids. This question was examined by changing the electrode surface treatment (mirror finish, rough finish) and the quantity of thermal bubbles (increased using a heater, reduced by pressurization). The volume effect was confirmed to be dominant in the large-scale electrode models, and the area effect mutually contributed to the volume effect in thermal bubble conditions, which would be a special correlation to cryogenic liquids with lower latent heat [7.9].

(b) Pressure dependence of breakdown strength

Figure 7.6 shows the ac breakdown strength in LN_2 for a sphere-to-plane electrode and a coaxial cylindrical electrode as a function of LN_2 pressure [7.9]. Breakdown strength for the coaxial cylindrical electrode is smaller than that for the sphere-to-plane electrode, which is attributed to the area and volume effect, i.e. the coaxial cylindrical electrode has the larger SEA and SLV by the order of 3 than those for the sphere-to-plane electrode.

Breakdown strength of the coaxial cylindrical electrode sharply rises with increasing pressure from 0.1 to 0.15 MPa, and saturates from 0.15 to 0.5 MPa. Since the coaxial cylindrical electrode has large SLV, there exist a lot of thermal bubbles in the gap space. Hence, breakdown in LN_2 may be triggered by discharge in bubbles at lower electric fields. When LN_2 is pressurized, the size and number of bubbles in LN_2 rapidly decrease. As a result, the breakdown strength sharply increases with pressure. When the pressure is further raised, almost all bubbles in LN_2 disappear. In such a condition, residual impurities become main weak points of breakdown in LN_2. These impurities remain in LN_2, irrespective of pressure, so that the breakdown strength in LN_2 saturates.

On the other hand, it is clear that the breakdown strength of the sphere-to-plane electrode gradually increases with pressure. For the sphere-to-plane electrode with small SLV, thermal bubbles in gap space cannot become main weak points of breakdown. Hence, breakdown may be triggered under higher electric field by discharge in small bubbles generated from micro-protrusions which enhance the local electric field strength on the electrode surface. When LN_2 is pressurized, the bubbles generated from the micro-protrusions are kept to a small size in the pressurized LN_2. As a result, the breakdown strength in LN_2 is not saturated but gradually increases with pressure.

(c) V-t characteristics at breakdown

V-t (voltage-time) characteristics play an important role in determining testing voltage level and estimating the lifetime of conventional power apparatus with a certain rated voltage. Figure 7.7 shows V-t characteristics at breakdown in LN_2 and LHe at atmospheric pressure for a coaxial cylindrical electrode [7.4]. Lifetime indices n of V-t

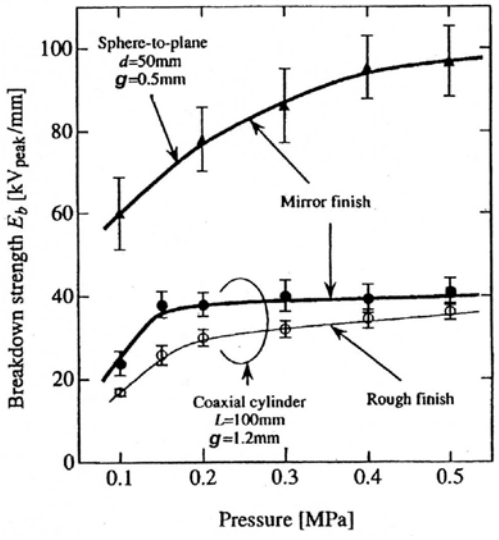

Fig. 7.6 Pressure dependence of breakdown strength in LN_2 [7.9]

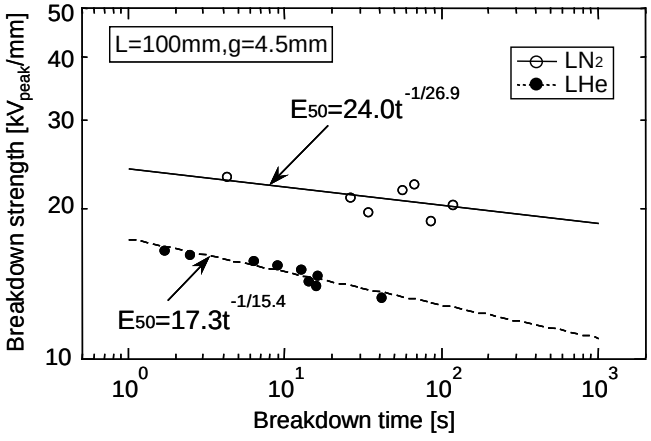

Fig. 7.7 V-t characteristics at breakdown in LN_2 and LHe [7.4]

characteristics at breakdown in LN_2 and LHe were 26.9 and 15.4, respectively. The difference in n values between LN_2 and LHe may be attributed to the difference in latent heat; i.e. LN_2 with higher latent heat than LHe has the longer lifetime because of the lower generation of thermal bubbles. In addition, n values for cryogenic liquids are smaller than n=38-58 for insulating oil [7.10].

(d) Quench-induced breakdown characteristics

One of the phenomena peculiar to superconducting power apparatus is the quench. The quench causes the generation and propagation of excessive voltage and heat in insulation materials. Hence, the quench-induced "dynamic" insulation characteristics in addition to the conventional "static" insulation characteristics should be understood for the reliable electrical insulation of superconducting power apparatus. The dynamic breakdown of LHe has been verified to take place with a lower voltage than the static breakdown voltage because of the quench-induced disturbance [7.11].

7.4 Dielectric Characteristics of HTS Power Cables

Most of the recent HTS cable projects use industrially produced HTS tapes which were insulated with solid dielectric tapes and impregnated with LN_2. Many different types of dielectric tapes were tested and used in prototype cables, including synthetic polymer. One of the most successful tapes is polypropylene (PP) laminated paper which is constructed like a sandwich. It joins the electrical, mechanical and thermal advantages of paper and the polymer PP with low dissipation factor, high electric strength, and good flexibility at LN_2 temperature. The PP laminated paper is wound on the conductor and butt gaps were necessary for mechanical flexibility. Under normal operating conditions these butt gaps were also filled with LN_2, but PD can occur in case of hotspots. The probability of PD can be reduced by higher operating pressure of LN_2. Taking account of the above factors, this section focuses mainly on the dielectric characteristics of LN_2/PP laminated paper composite insulation system for HTS cables.

7.4.1 Volume Effect on PD Inception Strength

PD inception characteristics of LN_2/PP laminated paper composite insulation system were investigated in terms of volume effect on PD inception electric field strength (PDIE) under ac voltage application. In order to discuss the PD inception characteristics and mechanisms of LN_2/PP laminated paper composite insulation system, a new parameter, statistical stressed liquid volume (SSLV), has been introduced [7.12]. SSLV is the parameter taking account of the discharge probability based on the electric field distribution, not only in the butt gap but also in LN_2-impregnated thin layers to be highly stressed between PP laminated paper layers caused by its own surface roughness. SSLV can be calculated by

$$SSLV = \iiint \left(\frac{E_i}{E_m} \right)^m dv$$

where E_i is the electric field strength at a volume unit i, E_m is the maximum electric field strength, and m is the Weibull shape parameter for PDIE, $(E_i/E_m)m$ corresponds to the relative PD probability at the volume unit i.

Figure 7.8 shows PDIE as a function of SSLV for different LN_2 pressures at 0.1 MPa and 0.2 MPa [7.13]. PDIE decreased linearly on a log-log plot with the increase in SSLV at SSLV < 100 mm^3 and was almost constant at SSLV > 100 mm^3. This result

suggests that the volume effect on PDIE was saturated at SSLV > 100 mm^3. The regression curve on PDIE at 0.2 MPa was shifted upward by 13-40 % from that at 0.1 MPa. The saturated PDIE at 0.1 MPa and 0.2 MPa were about 15 kV_{rms}/mm and 17 kV_{rms}/mm, respectively.

7.4.2 Pressure Dependence of PD Inception, Propagation and Breakdown Strength

Figure 7.9 shows the pressure dependence of PDIE for different numbers of insulating paper layers [7.14]. PDIE increased with the increase in the LN_2 pressure for all cases. This is because the pressurization of LN_2 suppresses the generation of microscopic bubbles and/or ionization of nitrogen molecules that are the cause of PD in LN_2. On the other hand, PDIE decreased with the increase in the number of insulating paper layers, which can be interpreted by the volume effect as described above. PDIE in the case of 48 layers at 0.3 MPa as the minimum LN_2 pressure of the 500 m HTS cable [7.15] is higher than 18 kV_{rms}/mm, which is consistent with the saturated PDIE on the volume effect in Fig. 7.8.

PD characteristics from its inception to breakdown were investigated with PD-CPWA, where the PD current pulse waveforms were successively obtained and statistically analyzed. As the result, PD generation frequency and PD current level drastically increased at a certain applied electric field strength (VDIE) higher than PDIE. Figure 7.10 shows the pressure dependence of PDIE, VDIE and BDE [7.16]. Through the

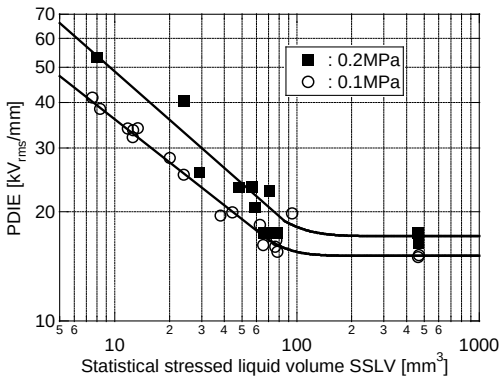

Fig. 7.8: PDIE as a function of SSLV [7.13]

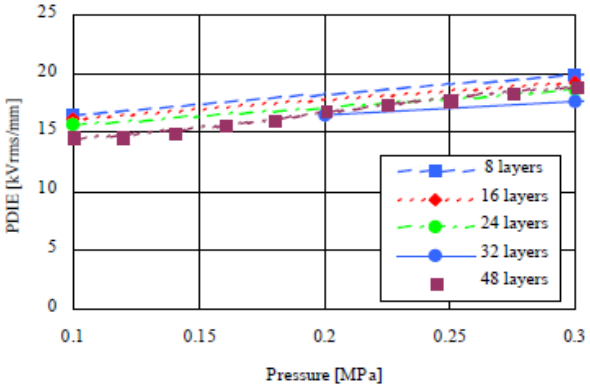

Fig. 7.9: Pressure dependence of PDIE [7.14]

observation of PD and breakdown traces, PD was verified to have been generated and developed in the butt gap area before breakdown. Under the reciprocal action of PD generation and bubble formation, the butt gap would be filled with bubbles to induce the void-type discharges, and finally lead to breakdown. Thus, the void-type discharge is an important electrical discharge form to characterize the transition of PD activity leading to breakdown, and its inception stress VDIE can be regarded as the electric field criterion for the electrical insulation design of HTS cables.

7.4.3 V-t Characteristics

For LN_2/PP laminated paper composite insulation system, V-t characteristics at PD inception as the precursor of breakdown were also investigated. This may be crucial to understand the insulation deterioration mechanism of the HTS cables. Figure 7.11 shows V-t characteristics at PD inception in LN_2/PP laminated paper composite insulation system [7.17]. The lifetime indices n at PD inception were as high as 80-

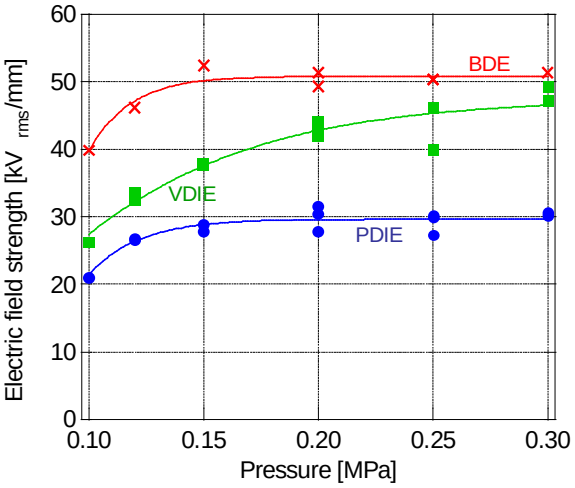

Fig. 7.10: Pressure dependence of PDIE, VDIE and BDE [7.16]

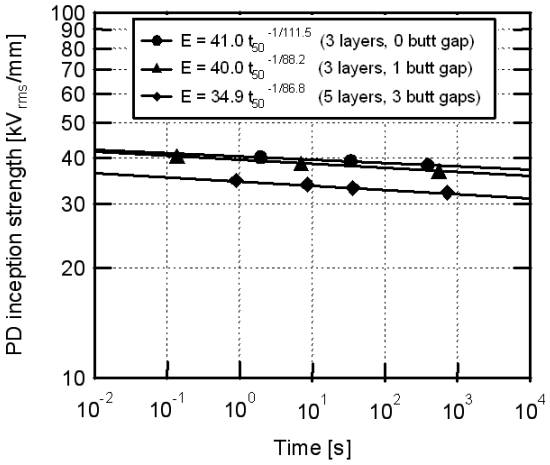

Fig. 7.11: V-t characteristics at PD inception in LN2/PP laminated paper composite insulation system [7.17]

100, irrespective of the butt gap conditions. In addition, n values at PD inception were higher than those at breakdown described above. The lower n values at breakdown can be interpreted by the intensified PD development in thermal bubbles in the butt gap after PD inception.

7.4.4 Quench-Induced PD Inception Characteristics

PD characteristics of HTS cables under quench condition are also crucial for the reliable insulation design, where the thermal stress due to quench can be transiently superposed on the electrical field stress under the operating voltage of HTS cables. Such electrical insulation characteristics under thermal/electrical combined stresses can be referred to as the “quench-induced PD characteristics” of HTS cables.

The quench-induced PD characteristics were investigated under a synthetic test circuit of 60 Hz ac high voltage and 60 Hz ac large current simultaneously applied to a test sample, i.e. with the test sample exposed to electric field stress, thermal stress due to quench is superposed for the pre-determined duration. Figure 7.12 shows typical example of quench-induced PD characteristics for a test sample with coaxial cable configuration composed of HTS tapes and PP laminated papers [7.18]. PD signal was detected after the current injection, i.e. quench of HTS tapes, with the delay time of about 120 ms. The delay time would correspond to the time from the quench of HTS tapes to the bubble formation in the insulation layers through heat transfer in semiconducting sheets between HTS tapes and PP laminated papers. The microscopic bubble would trigger the first PD, and the first PD would induce more bubbles to activate PD generation. Such a positive feedback of bubble formation and PD generation could result in the void-type discharge pattern in Fig. 7.12 until the bubbles disappeared.

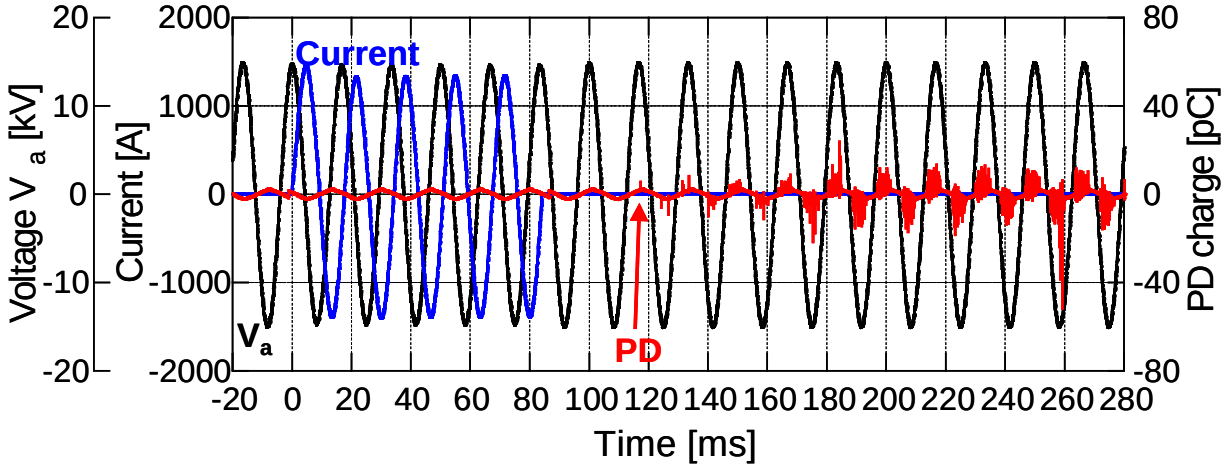

Fig. 7.12: Quench-induced PD characteristics [7.18]

The pressure dependence of quench-induced PD characteristics is shown in Fig. 7.13 for different LN_2 pressures P=0.1 MPa, 0.12 MPa, 0.15 MPa and 0.2 MPa, respectively. The quench-induced PD activity such as PD charge and PD duration was suppressed with the increase in pressure from 0.1 MPa to 0.2 MPa, which is attributed to the suppression of bubble formation and propagation in sub-cooled LN_2. Figure 7.14 shows the criterion for quench-induced PD inception for different LN_2 pressures as functions of the normalized stresses $V_a/PDIV_{sta}$ and I_{1st}/I_c [7.18]. With the increase in LN_2 pressure, the boundary curve of quench-induced PD inception

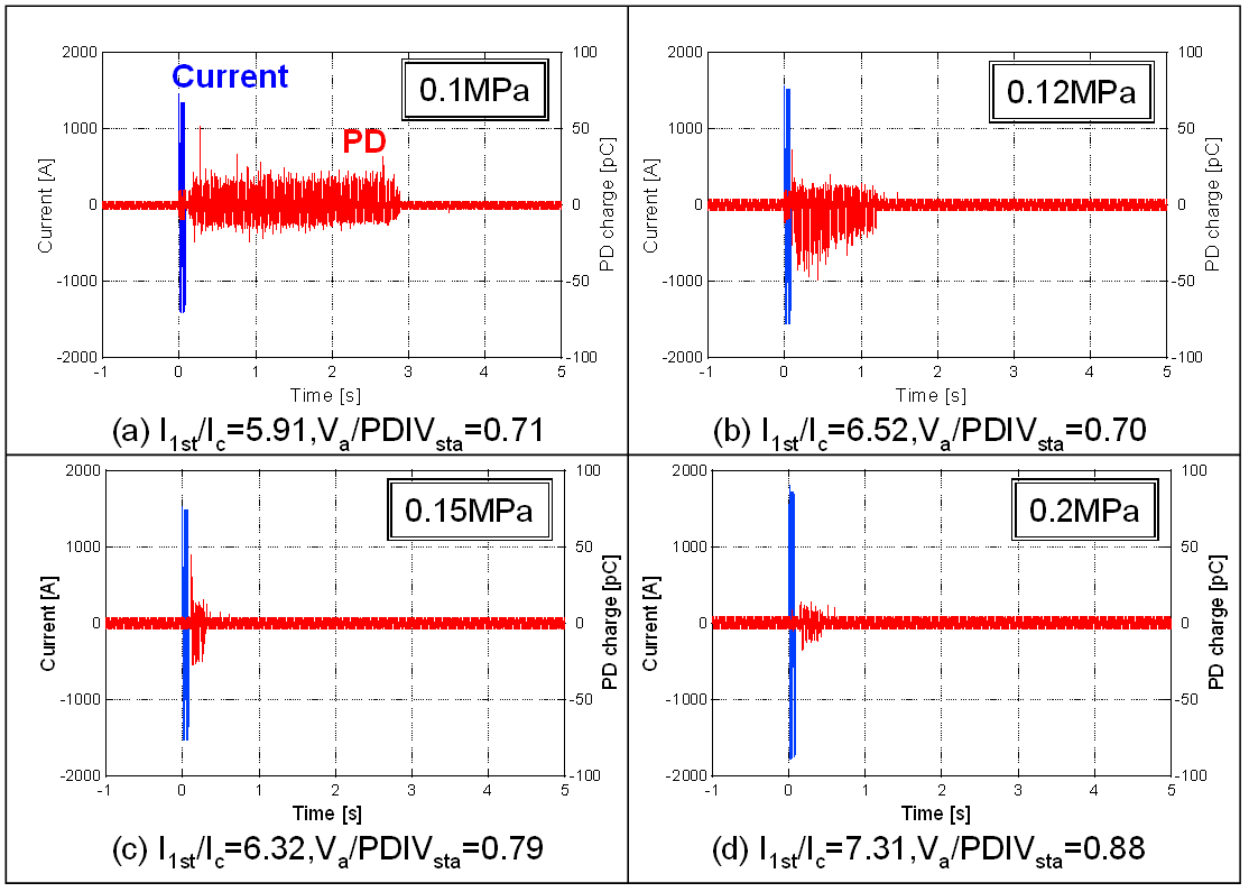

Fig. 7.13: Pressure dependence of quench-induced PD characteristics [7.18]

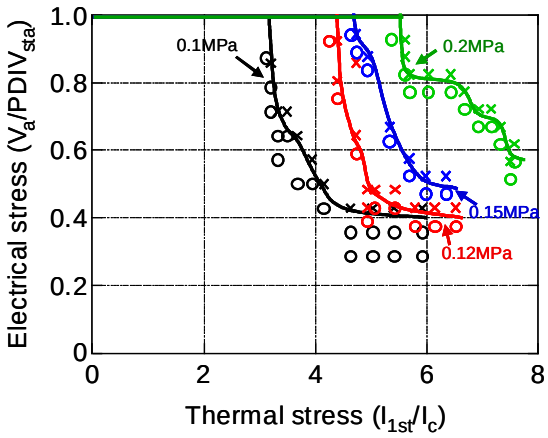

Fig. 7.14: Criteria of quench-induced PD inception [7.18]

shifted toward the higher stress region, i.e. the higher PD inception strength is expected against the thermal/electrical combined stresses. However, V_a/PDIV$_{sta}$ would decrease into 0.4-0.5 at P=0.1-0.2 MPa, when the thermal stress could reach I_{1st}/I_c=6-7.

7.5 Dielectric Characteristics of HTS Fault Current Limiters and Transformers

Electrical insulation system of fault current limiters and transformers will be exposed to non-uniform electric field, e.g. coils edges and different combinations of solid, liquid, gas and vacuum dielectrics, as can be seen in Fig. 7.15 [7.19]. Thus, in general, the electrical insulation of HTS fault current limiters and transformers is more complicated than that of HTS cables exposed to the quasi-uniform electric field of a coaxial cylindrical configuration. Especially, technical difficulties of cryodielectrics can be found in cracks in solid dielectrics, bubbles in liquid dielectrics, surface discharges on solid dielectrics in vacuum, and so on. This section introduces some topics on the dielectric characteristics of HTS coils for fault current limiters and transformers.

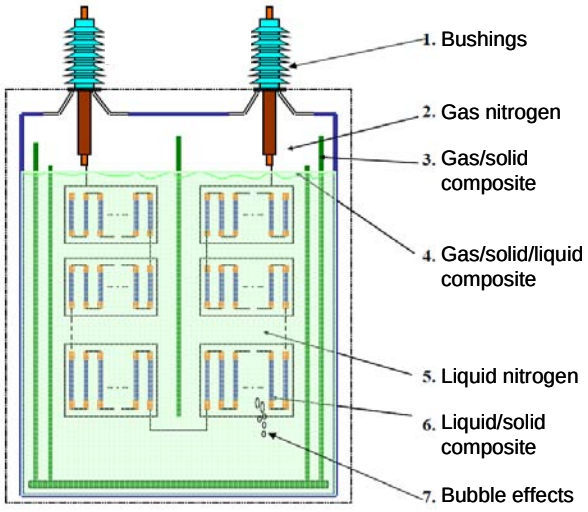

Fig. 7.15: Electrical insulation system of fault current limiters [7.19]

7.5.1 Fundamental Dielectric Characteristic of HTS Coil

For the electrical insulation of HTS coils, turn-to-turn and layer-to-layer insulation characteristics should be understood. Furthermore, in order to enhance the electrical insulation and cooling performance, dielectric characteristics of sub-cooled LN_2 are important.

Figure 7.16 shows the breakdown voltage as a function of turn-to-turn distance of a model coil for a 66 kV HTS fault current limiter [7.20]. The breakdown characteristics of sub-cooled LN_2 at 65 K were almost the same as those of LN_2 at 77 K under both ac and lightning impulse voltages. The breakdown voltage under lightning impulse (solid line) was about 1.2 times higher than that under ac voltage (broken line). In addition, the breakdown characteristics in a mixture of LN_2 and bubbles generated by a heater were investigated. The breakdown voltage was considerably improved in sub-cooled LN_2 at 65 K: it was as high as twice that in LN_2 at 77 K.

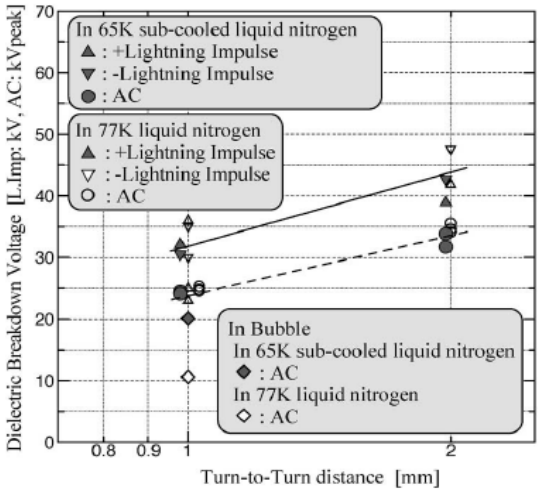

Fig. 7.16: Breakdown voltage as a function of turn-to-turn distance of a model coil for the 66 kV HTS fault current limiter [7.20]

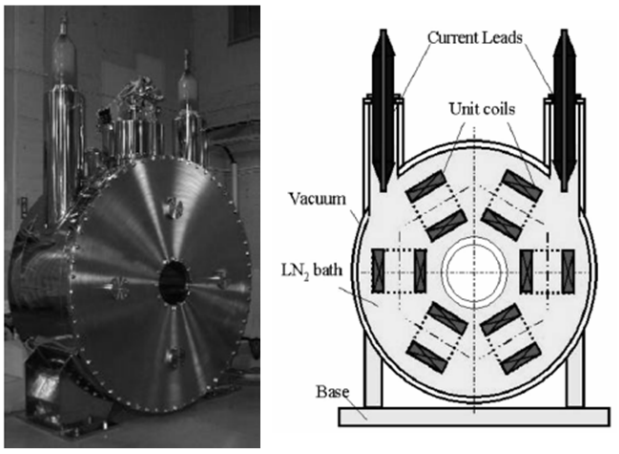

Fig. 7.17: Photograph and schematic drawing of the 66 kV HTS fault current limiter [7.21]

Figure 7.17 shows a photograph and schematic drawing of the 66 kV HTS fault current limiter developed by Toshiba, with 6 coils connected in series [7.21]. The withstand voltage of 140 kV_{rms} in ac voltage and 350 kV_{peak} in lightning impulse voltage was verified in sub-cooled LN_2 at 70 K under atmospheric pressure.

7.5.2 Quench Induced PD and Breakdown Characteristics

The quench-induced PD characteristics, as was shown in section 7.4.4 for HTS cables, can also be applied to HTS fault current limiters of resistive type utilizing quench of HTS materials. The quench-induced PD inception and breakdown (BD) characteristics for an epoxy-impregnated electrode system in LN_2 have been discussed [7.22]. A pair of ring electrodes molded with epoxy resin was immersed in LN_2 to simulate the fault current limiter coil, and exposed to thermal/electrical combined stresses. The thermal stress simulating the quench of HTS materials was transiently applied to the ring electrodes by the electromagnetic induction current. Figure 7.18 shows the electrical insulation performance under electrical/thermal combined stresses, where the horizontal axis represents the estimated maximum temperature of the ring electrode [7.22]. There exists a criterion designated by a solid curve to discriminate PD and/or BD region from a region with no PD or BD. This criterion has been reflected to the insulation design of 10 MVA HTS fault current limiter [7.23].

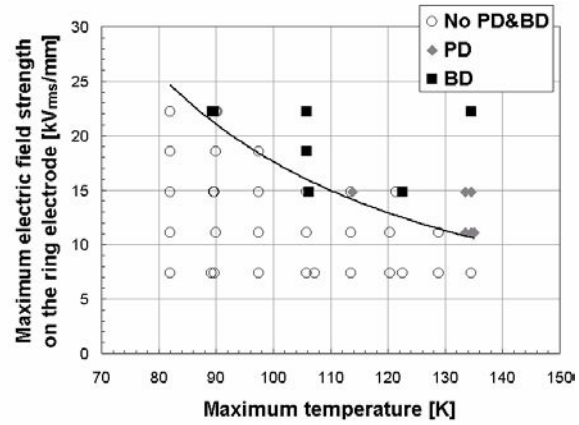

Fig. 7.18: Electrical insulation performance under electrical/ thermal combined stresses [7.22].

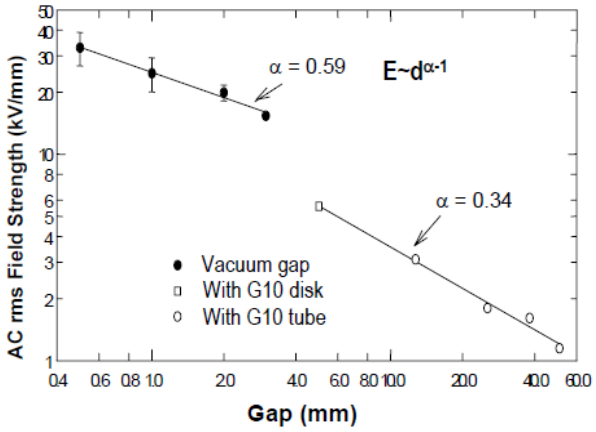

Fig. 7.19: AC breakdown field strength of vacuum gap and G-10 spacers as a function of gap length at room temperature [7.24]

Dielectric strength in vacuum

Electrical insulation of HTS power apparatus will follow either of two design paths: solid insulation immersed in LN_2 or vacuum insulation with solid spacers. The former solid insulation has been mainly dealt in the previous sections. The latter vacuum insulation will be focused on in this section, for e.g. conduction-cooled HTS coils.

Figure 7.19 shows the ac breakdown field strength of pure vacuum gap and fiberglass reinforced plastics (FRP, G-10) spacers as a function of gap length at room temperature [7.24]. The G-10 spacer has the disk or tube configuration, and the fibers are oriented perpendicular to the electric field. All breakdowns were not puncture, but flashover along the disk surface. The surface flashover strength on G-10 spacers was much lower than the breakdown strength of vacuum gap. The breakdown strength at 90 K was about 30 % lower than that at 293 K for a 2 mm vacuum gap. However, in the case of surface flashover on G-10 disk with 5 mm thickness, there was very little temperature dependence of surface flashover voltage, which may be attributed to the outgassing of G-10, i.e. electron impact desorption of condensed gases from the dielectric surface. Other researchers have observed little or no difference between room temperature and 100 K for polycarbonate [7.24]. The significant decrease in flashover strength with insulation length indicates that experimental data are needed on large bridged vacuum gaps at cryogenic temperatures, not only for FRP, but for other dielectric materials as well, for designing large scale HTS power apparatus.

7.6 Conclusions

The state-of-the-art activities in research and development on cryodielectrics were introduced in this brief review. There are still many factors to be discussed and elucidated for the reliable, practical and rational insulation design of HTS power apparatus. Intensive and successive research activities on cryodielectrics are expected with understanding of the physical mechanisms of PD inception, propagation and breakdown at cryogenic temperature.

8 Summary

The main purpose of this report was to summarize the state-of-the-art and the field test experience with high temperature superconductor power devices.

Superconductor materials for wire-based power applications are making rapid progress. Active competition continues between different materials, and different forms of these materials; the long-term winners are not yet clear, and each material may yet find its niche. But overall prospects for superconductors impacting the power grid have never been brighter. It is likely that the so-called 2nd generation HTS wires based on YBCO can beat the cost-performance ratio of copper.

Several prototypes of rotating electrical machines from a few MW up to 36 MW with HTS rotor windings have been successfully built and tested. A range of applications, including ship propulsion motors, utility generators, wind turbine generators and synchronous condensers are all being explored. It can be expected that within the next decade, the first commercial applications of superconducting rotating machines will be in the market. The only rotating machine so far tested in a real utility environment is a dynamic synchronous condenser.

HTS cable projects are actively pursued around the world, making HTS cable one of the most promising and likely commercial power grid applications. Key technical issues have been solved, making both distribution and transmission-level cables a realistic possibility. And with multiple cables in operation in utility grids, reliability is being demonstrated. Almost all cable systems currently under consideration are of the cold dielectric design, which offers the full range of functional benefits of HTS cables. Additionally, 1G HTS wire (Bi-2223) is increasingly being replaced by 2G (YBCO) as the conductor of choice for HTS cables, due to its lower cost potential. The use of 2G wire is also opening a new avenue for HTS cable systems - a cable with inherent fault current limiting.

At present, many projects worldwide are on their way to develop prototype SCFCLs for further field tests, and the first superconductor fault current limiters (SCFCLs) are becoming commercially available . Although there are different types of SCFCLs, most of the projects increasingly follow the resistive-type design, and recently more and more projects use 2G HTS wire (YBCO coated conductor) as the superconductor of choice. While at distribution voltage levels all technical issues have been demonstrated, the major challenge is cost reduction. There is another major challenge for transmission voltage SCFCFL - to demonstrate reliable high voltage insulation.

A SMES unit stores and discharges DC power at efficiencies of 98% or more and can switch between charging and discharging within milliseconds. Several SMES devices have been successfully operating since 1998, for power quality and system stability applications. At present, commercially available SMES systems still use LTS but HTS applications are being developed. Major challenges for the HTS SMES include achieving competitive energy density and cost.

HTS transformers offer significant potential benefits, but lack of a practical, low-ac-loss conductor has limited progress up to now. While projects in the US (SuperPower and Waukesha; American Superconductor, ABB and EDF) and Europe (Siemens traction transformer) have terminated, work is progressing in Japan and

China, and progress is being made on low-ac-loss conductor with 2G HTS wire. A concept for a fault current limiting transformer was described.

Liquid nitrogen acts simultaneously as a coolant and dielectric liquid in many HTS power devices. The breakdown properties are excellent and can be compared with transformer oil. Since the breakdown voltage of gaseous nitrogen is reduced in comparison to liquid nitrogen, bubble nucleation must be suppressed. For the reliable electrical insulation design of HTS power equipment, partial discharge (PD) inception and propagation activities are to be investigated in GN_2, LN_2 and their composite system with solid materials. The chemical inertness of liquid nitrogen reduces the fire and contamination risk even in case of failures.

In summary, rapid progress is being made in developing and field-testing HTS electric power equipment. Based on this progress, one can expect significant impact on the grid around the world during the next decade.

9 References

Section 1 Introduction

[1.1] MUELLER K, BEDNORZ G, Z. Physik B., Condensed matter 64, 189-193, 1986

[1.2] CIGRE Paper No. D1-403: Technical Trend of Superconducting and Electrical Insulating Materials for HTS Power Applications, By WG SC D1.15, 2004

[1.3] CIGRE Paper No. D1-306: Development and Application Trend of Superconducting Materials and Electrical Insulation Techniques for HTS Power Equipment, By WG SC D1.15, 2006

[1.4] KALSI S, et. al, Proceedings IEEE, Vol. 92, No.10, October, 2004

[1.5] WOLSKY A, IEA Report December, 2004

[1.6] MCCONNEL B, MEHTA S, WALKER M, HTS Transformers IEEE Power Engineering Review June, 2000

[1.7] NOE M and STEURER M 2007 Supercond. Sci. Technol. 20, R15-R29, 2007

[1.8] BUCKLES W, HASSENZAHL W, Superconducting magnetic energy storage, IEEE Power Engineering Review May, 2000

[1.9] MALOZEMOFF A et. al. Supercond. Sci. Technol. 21, 034005 (7pp), 2008

Section 2 Materials

[2.1] SCANLAN R M et al., Proc. of IEEE 92, 1639-54, 2004.

[2.2] SATO K, FSST 33rd Symposium, Tokyo, Japan, April 17, 2007; S. Kobayashi et al., IEEE Trans. on Applied Superconductivity 15, 2534-7, 2005.

[2.3] MALOZEMOFF A P , IEEE Trans. on Applied Superconductivity 16, 54-59, 2006.

[2.4] KOIZUMI T et al., IEEE Trans. on Applied Superconductivity 15, 2538-41, 2005.

[2.5] MIAO H et al., IEEE Trans. on Applied Superconductivity 15, 2554-57, 2005.

[2.6] NAGAYA S et al., CIGRE Session 15-403, 2002.

[2.7] AOKI Y et al., in Advances in Superconductivity XII, T. Yamashita and K. Tanabe, eds. (Springer Verlag, Tokyo, Japan), pp. 827-829, 2000

[2.8] HELLSTROM E E and ZHANG W, in Bismuth Based High Temperature Superconductors, H. Maeda and K. Tagano, eds. (Marcel Dekker, new York, pp. 427-449, 1995.

[2.9] BOCK J et al., IEEE Trans. on Applied Superconductivity 3, 3145-8, 1993.

[2.10] CARRASCO M F, Superconductor Sci. Tech. 19, 373-380, 2006.

[2.11] SAGER D et al., Physica C 420, 69-77, 2002.

[2.12] BUHL D et al. Supercond. Sci. Technol. 10, 32-40, 1997.

[2.13] MAEDA H et al., Physica C 386, 115-121, 2003.

[2.14] GLOWACKI B A et al., Physica C 384, 205-210, 2003.

[2.15] NATIVIDAD E et al., Supercond. Sci. Technol. 17, 308-313, 2004.

[2.16] BOCK J et al., IEEE Trans. on Applied Superconductivity 15, 1955-60, 2005.

[2.17] MAJEWSKI P et al., J. Mater. Res. 15, 854-870, 2000.

[2.18] BOCK J et al., IEEE Trans. on Applied Superconductivity 5, 1409-1412, 1995.

[2.19] ANGUREL L A et al., Supercond. Sci. Technol. 18, 135-141, 2005.

[2.20] YUAN X et al., IEEE Trans. on Applied Superconductivity 15, 1982-5, 2005.

[2.21] CHEN M, Physica C 372-6, 1657-63, 2002.

[2.22] HYUN O B et al., KEPRI, to be published.

[2.23] RUPICH M et al., presented at Applied Superconductivity Conference, Seattle WA Aug. 28-Sept. 1, 2006, and MALOZEMOFF A., presented at CIGRE Workshop, Nagoya Japan, May 13-14, 2009.

[2.24] PETERSON D E, presented at 19th International Symposium on Superconductivity, Nagoya Japan, Oct. 30-Nov. 1, 2006.

[2.25] SHIOHARA Y et al., presented at 19th International Symposium on Superconductivity, Nagoya Japan, Oct. 30-Nov. 1, 2006.

[2.26] SELVAMANICKAM V et al., presented at 19th International Symposium on Superconductivity, Nagoya Japan, Oct. 30-Nov. 1, 2006, and presented at 2008 DOE High Temperature Superconductivity Program Peer Review, Arlington VA, July 29-31, 2008.

[2.27] TAKAHASHI Y et al., presented at 19th International Symposium on Superconductivity, Nagoya Japan, Oct. 30-Nov. 1, 2006.
[2.28] FREYHARDT H, presented at 19th International Symposium on Superconductivity, Nagoya Japan, Oct. 30-Nov. 1, 2006.
[2.29] NEUMUELLER H-W et al., presented at IEEE PES General Meeting, Tampa FL, June 24-28, 2007.
[2.30] private communication, to be published.
[2.31] MAGUIRE J et al., presented at 2007 US DOE Annual Peer Review, Superconductivity for Electric Systems, Washington DC, Aug. 7-9, 2007.
[2.32] SELVAMANICKAM V, presented at 2007 US DOE Annual Peer Review, Superconductivity for Electric Systems, Washington DC, Aug. 7-9, 2007.
[2.33] NAGAMATSU J et al., Nature 410, 63-4, 2001.
[2.34] TANAKA K et al., IEEE Trans. on Applied Superconductivity 15, 3180-4, 2005.
[2.35] SERQUIS A et al., IEEE Trans. on Applied Superconductivity 15, 3188-91, 2005.
[2.36] BRACCINI V et al., IEEE Trans. on Applied Superconductivity 15, 3211-4, 2005.
[2.37] BHATIA M et al., IEEE Trans. on Applied Superconductivity 15, 3204-7, 2005.
[2.38] YE L et al., Supercond. Sci. Technol. 20, 621-8, 2007.
[2.39] Press release, Bruker HTS, Bruker HTS and Nexans announce successful completion of European Superconducting Cable Project, March 17, 2009
[2.40] MUKOYAMA S et. al. Presented at 21th International Symposium on Superconductivity (ISS2008), Tsukuba Japan (2008) SA-5-INV, 2008
[2.41] HAYAKAWA N et al., CIGRE HTS Workshop in Nagoya, May, 2009

Section 3 Machines

[3.1] KALSI S, et al, American Superconductor, Naval Symposium on Electrical Machines, Annapolis MD, October 26-29, 1998.
[3.2] KALSI S, et al, Naval Symposium on Electric Machines, Philadelphia, PA on December 4-7, 2000
[3.3] ECKELS P and SNITCHER G, Naval Symposium on Electric Machines, Philadelphia, PA on January, 2004.
[3.4] WEEBER K K, et al, presented at the IEEE 2003 Power Engineering Society Annual Meeting, Emerging Technologies Panel Session, Toronto, ON, Canada
[3.5] WACKER B, SCHMIDT W and ANDERSEN P, presented at the All Electric Ship Conference, Edinburgh, U.K., 2003
[3.6] WOODRUF S , et al, presented at IEEE Electric Ship Technologies July 2005 Philadelphia.
[3.7] GAMBLE B B, IGE S O, ALEXANDER D and RICKET R, presented at ASNE symposium, May 2006
[3.8] KALSI S, GAMBLE B, SNITCHLER G and IGE S O presented at the IEEE PES in Montreal, May 20, 2006.
[3.9] FRAUENHOFER J et al., Proceedings of the International Conference Ship Propulsion and Railway Traction Systems, Bologna, Italy, Oct. 2005
[3.10] NEUMUELLER H-W et al., Proceedings of the AES 2005, Paris/Versailles, France, Oct. 2005
[3.11] NEUMUELLER H-W et al., Supercond. Sci. and Technol. No. 19, pp. 114-117, 2006
[3.12] NICK W et al., HTS – Propulsion machines – results and future, Proceedings of the WMTC Technology Conference, London, UK, March 2006
[3.13] FRAUENHOFER J et al., Proceedings of the SPEEDAM Symposium, Taormina, Italy, May 2006
[3.14] NEUMUELLER H-W et al.,Proceedings of the CIMTEC 2006, Sicily, Italy, June 2006
[3.15] KLAUS G et al., IEEE Power Engineering Society, Gen. Meeting, Montreal, Canada, June 2006
[3.16] KALSI S et al., IEEE Trans. on Applied Superconductivity 17, No. 2, 1591-4, 2007.
[3.17] KLAUS G et al., Proceedings of the 2007 IEEE PES General Meeting, Tampa, FL, USA, June 2007.
[3.18] FRAUENHOFER J et al., Proceedings of the 2007 European Conference on Applied Superconductivity – EUCAS 2007, Brussels, Belgium, September 2007.
[3.19] BUCK J et al., Proceedings of the 2007 ASNE Day Symposium, Arlington, VA, USA, June 2007.

[3.20] KWON Y K et al., Proceedings of the 2007 IEEE PES General Meeting, Tampa, FL, USA, June 2007.
[3.21] FOGARTY J M presented at the IEEE 2004 PES Annual Meeting, 2004
[3.22] LEWIS C and MUELLER J, Proceedings of the 007 IEEE PES General Meeting, Tampa, FL, USA, June 2007.
[3.23] OKAZAKI T et al., Proceedings of the 2006 IEEE PES General Meeting, Montréal, Canada, June 2006.
[3.24] SUMITOMO ELECTRIC Inc. “Development of World's Most Powerful Liquid-Nitrogen-Cooled BSCCO Superconducting Motor”, Press Release, September 3, 2007.
[3.25] SIVASUBRAMANIAM K et al., Proceedings of the 2007 IEEE PES General Meeting, Tampa, FL, USA, June 2007.
[3.26] Siemens “Ice-cold continuous operation at -243 degree celsius”, Press Release, April 16, 2009

Section 4 Cables

[4.1] MUKOYAMA S, et al, IEEE Trans. on Applied Superconductivity, Vol. 17, No. 2, June 2007
[4.2] TORII S, et al, IEEE Transactions on Applied Superconductivity, Vol. 17, No. 2, June 2007
[4.3] ICHIKAWA M, et. Al. , IEEE Trans. on Applied Superconductivity, Vol. 17, No. 2, June 2007
[4.4] MAGUIRE J F, et al, IEEE Trans. on Applied Superconductivity, Vol. 17, No. 2, June 2007
[4.5] WEBER C C, et al., IEEE Trans. on Applied Superconductivity, Vol. 17, No. 2, June 2007
[4.6] DEMKO J A, et al., IEEE Trans. on Applied Superconductivity, Vol. 17, No. 2, June 2007
[4.7] YING Y, et al IEEE Trans. Applied Superconductivity, Vol. 15, No. 2, Part 2, 1814 – 1817, June 2005
[4.8] YAMAGUCHI S, et al., Journal of Physics, Conference Series 97, 012290, 2008

Section 5 Superconducting Fault Current Limiters

[5.1] PAUL W et al., Inst. Phys. Conf. Ser. 158 1173-1178, 1997
[5.2] KREUTZ R et al., IEEE Trans. Applied Superconductivity 15 No 2 1961-1964, 2005
[5.3] BOCK J et al., IEEE Trans. Applied Superconductivity 15 No 2 1955-1960, 2005
[5.4] WANG Z K et al., IEEE Trans. Applied Superconductivity 16 No 2 658 – 661, 2006
[5.5] HUI D et al., IEEE Trans. Applied Superconductivity. 16 No 2 687-690, 2006
[5.6] NOE M and STEURER M Supercond. Sci. Technol. 20 R15-R29, 2007
[5.7] ELSCHNER S et al., IEEE Trans. Applied Superconductivity 13 No 2 1980-1983, 2003
[5.8] SUPERCONDUCTOR WEEK Chinese Academy of Sciences demonstrate HTS fault current limiter Superconductor Week 19 No 24, 2005
[5.9] BOENIG H J and PAICE D A IEEE Transactions on Magnetics 19 No 3 1051-1053, ,1983
[5.10] SCHMIDT W et al., IEEE Trans. on Applied Superconductivity (Seattle) 17 No 2 3471-74, 2007
[5.11] KRAEMER H-P et al., Proc. of the EUCAS2007 (Brussels, 2007, Oct. 17. – 20.), 2007
[5.12] MARTINI L et al., CIRED 2005, 18th Int. Conf. on Electricity Distribution, Turin 6-9 June, Session No 1, Paper 0533, 2005.
[5.13] DALESSANDRO R B et al., IEEE Trans. on Applied Superconductivity, Vol. 17, No. 2, Part 2, pp. 1776 - 1779, 2007.
[5.14] NARDELLI D et al., IEEE Trans. on Applied Superconductivity, Vol. 17, No. 2, Part 3, pp. 2742 - 2745, 2007.
[5.15] MARTINI L et al., CIGRE General Session, Paper D1-302, Paris (F), 27 August 2006.
[5.16] YE L et al., IEEE Trans. on Applied Superconductivity, Vol. 17, No. 2, Part 3, pp. 2826 - 2829, 2007.
[5.17] HAYAKAWA N et al., Proc. 8th European Conference on Applied Superconductivity, 16-20 Sept. 2007, Brussels, Sept. 2007
[5.18] KURUPAKORN C et al., IEEE Trans. on Applied Superconductivity Vol.14, No.2, pp.900-903, 2004.
[5.19] KURUPAKORN C et al., IEEE Trans. on Applied Superconductivity Vol.15, No.2, pp.1859-1862, 2005.
[5.20] KURUPAKORN C et al., Journal of Physics: Conference Series, Vol.43, pp.950-953, 2006.
[5.21] OKUBO et al., IEEE Trans. on Applied Superconductivity, Vol.17, No.2, pp.1768-1771, 2007.

[5.22] SEOK B Y et al, presented at Magnet Technology Conference MT 20, 27-31 August 2007 Philadelphia, to be published in IEEE Trans. Applied Superconducivity, 2007
[5.23] YAZAWA T, Proc. 8th European Conference on Applied Superconductivity, 16-20 Sept. 2007, Brussels, Sept 2007
[5.24] LEE B W et al., Proc. 8th European Conference on Applied Superconductivity, 16-20 Sept. 2007, Brussels, Sept 2007.
[5.25] ENDO M et al., Proc. 8th European Conference on Applied Superconductivity, 16-20 Sept. 2007, Brussels, Sept 2007.
[5.26] HORI T et al., IEEE Trans. Applied Superconductivity Vol. 16 No. 4, pp 1999-2004, Dec. 2006
[5.27] XING Y et al., IEEE Trans. Applied Superconductivity Vol. 15, No. 2, pp. 1982-1985, June 2004
[5.28] XIE Y Y et al., IEEE Trans. Applied Superconductivity Vol. 17, No. 2, pp 1981-1985, June 2007
[5.29] ELSCHNER S et al., IEEE Trans. Applied Superconductivity Vol. 17 No. 2, pp 1772-1775, June 2007
[5.30] ELSCHNER S et al., Proc. 8th European Conference on Applied Superconductivity, 16-20 Sept. 2007, Brussels, Sept. 2007.
[5.31] DOE press release 2007

Section 6 Superconducting Magnetic Energy Storage

[6.1] MOON F C, Journal Applied Physics, vol. 53, pp. 9112-9121, 1982.
[6.2] LUONGO C A IEEE Transactions on Magnetics, vol. 32, pp. 2214-2223, 1996.
[6.3] JUENGST K-P, KUPERMAN G, 2nd European Pulsed Power Symposium, Hamburg, Germany, Sept. 2004.
[6.4] NAGAYA S, et. al. IEEE Trans. on Applied Superconductivity Volume 14, Issue 2, pp. 699 – 704, June 2004.
[6.5] NAGAYA S, et. al. , IEEE Trans. on Applied Superconductivity, Volume 16, Issue 2, pp. 632 – 635, June 2006.
[6.6] TIXADOR P, et. al. IEEE Trans. on Applied Superconductivity, vol. 17, pp. 1707-1710, 2007.
[6.7] FLAHAUT E, et.al. , IEEE Trans. on Applied Superconductivity, vol. 13, pp. 3034 – 3037, 2003.
[6.8] Hasegawa T. et. al., IEEE Trans. on Applied Superconductivity, Vol.12, No.1, pp. 1 136, 2002.
[6.9] NAGAYA S, et. al.,"Development of the Bi-2212Superconductor for high voltage magnets andevaluation of the temperature and magnetic stability,"Session-2002, Cigre, 15-403, ,2002.
[6.10] SHIKIMACHI K, et. al., IEEE Trans. on Applied Superconductivity, Vol. 15, No. 2, pp. 1931-1934, June 2005.
[6.11] SHIKIMACHI K, et. al., IEEE Trans. on Applied Superconductivity, Vol. 17, No. 2, pp. 2220-2223, June 2007.

Section 7 Electrical Insulation

[7.1] SCHWENTERLY W, Cryogenic Dielectrics Workshop, Nashville, USA, 2005
[7.2] http://www.energetics.com/meetings/supercon04/pdfs/summaries/spi_b_schwenterly_pleva_hazelton.pdf
[7.3] MITO T, et al., IEEE Trans. on Applied Superconductivity, Vol.17, pp.1973-1976, 2007
[7.4] OKUBO H, et al., IEEE Trans. on Power Delivery, Vol.11, No.3, pp.1400-1406, 1996
[7.5] GERHOLD J, IEEE Trans. on Dielectrics and Electrical Insulation, Vol.9, No.6, pp.878-890, 2002
[7.6] SUMEREDER C, MUHR M, WOSCHITZ R, Int. Conf. on Properties and Applications of Dielectric Materials (ICPADM), pp.506-509, 2003
[7.7] FRAYSSINES P E, LESAINT O, et al.,IEEE Trans. DEI, Vol.9, No.6, pp.899-909, 2002
[7.8] OKUBO H and HAYAKAWA N, IEEE Trans. on Dielectrics and Electrical Insulation, Vol.12, No.4, pp.736-744, 2005
[7.9] HAYAKAWA N, et al., IEEE Trans. on Dielectrics and Electrical Insulation, Vol.4, No.1, pp.127-134, 1997
[7.10] IKEDA M, YANARI T, OKUBO H, IEEE Trans. on Power Apparatus and Systems, Vol.101, No.8, pp.2728-2735, 1982

[7.11] CHIGUSA S, HAYAKAWA N, OKUBO H, IEEE Trans. on Dielectrics and Electrical Insulation, Vol.7, No.2, pp.290-295, 2000

[7.12] HAYAKAWA N, et al., IEEE Trans. on Dielectrics and Electrical Insulation, Vol.12, No.1, pp.166-174, 2005

[7.13] HAYAKAWA N, et al., IEEE Trans. on Applied Superconductivity, Vol.15, No.2, pp.1802-1805, 2005

[7.14] SUZUKI H, et al., 7th Int. Conf. on Properties and Applications of Dielectric Materials (ICPADM), pp.1182-1185, 2003

[7.15] MUKOYAMA S, et al., IEEE Trans. on Applied Superconductivity, Vol.17, pp.1680-1683, 2007

[7.16] OKUBO H, et al., 15th Int. Symp. on High Voltage Engineering (ISH), T3-113, 2007

[7.17] OKUBO H, HAZEYAMA M, HAYAKAWA N, HONJO S, MASUDA T, IEEE Trans. DEI, Vol.9, No.6, pp.945-951, 2002

[7.18] HAYAKAWA N, et al., 8th European Conference of Applied Superconductivity (EUCAS), L2-0080, 2007

[7.19] TEKLETSADIK K, Cryogenic Dielectrics Workshop, Nashville, USA, 2005

[7.20] KOYAMA H, et al., IEEE Trans. on Applied Superconductivity, Vol.14, No.2, pp.1181-1184, 2004

[7.21] YAZAWA T, et al., IEEE Trans. on Applied Superconductivity, Vol.16, No.2, pp.683-686, 2006

[7.22] HAYAKAWA N, et al., IEEE Trans. on Applied Superconductivity, Vol.13, No.2, pp.1996-1999, 2003

[7.23] NOE M, et al., IEEE Trans. on Applied Superconductivity, Vol.15, No.2, pp.2082-2085, 2005

[7.24] SAUERS I, et al., IEEE Trans. on Dielectric and Electrical Insulation, Vol.9, No.6, pp.922-931, 2002

[7.25] NEUBER A, KROMPHOLZ H, HATFIELD L L, Conference on Electrical Insulation and Dielectric Phenomena (CEIDP), pp.575-578, 1997

[7.26] OKUBO H, et al., CIGRE HTS Workshop in Nagoya, May, 2009